UNIVERSIDAD DEL VALLE

DEGREE THESIS

Magnetic properties of spinor boson gases in optical lattices: a Gutzwiller variational approach

---

Author:
Gustavo MARÍN

Supervisor:
Dr. Karem RODRÍGUEZ

A thesis submitted in fulfillment of the requirements for the degree of Degree Thesis as Physicist

in the

Física Teórica del Estado Solido
Departmento de Física
Facultad de Ciencias Naturales y Exactas
Universidad Del Valle
Cali, Colombia

May 11, 2019

Declaration of Authorship

I, Gustavo MARÍN, declare that this thesis titled, "Magnetic properties of spinor boson gases in optical lattices: a Gutzwiller variational approach " and the work presented in it are my own. I confirm that:

- This work was done wholly or mainly while in candidacy for a degree at this University.
- Where any part of this thesis has previously been submitted for a degree or any other qualification at this University or any other institution, this has been clearly stated.
- Where I have consulted the published work of others, this is always clearly attributed.
- Where I have quoted from the work of others, the source is always given. With the exception of such quotations, this thesis is entirely my own work.
- I have acknowledged all main sources of help.
- Where the thesis is based on work done by myself jointly with others, I have made clear exactly what was done by others and what I have contributed myself.

Signed:

Date:

UNIVERSIDAD DEL VALLE

Abstract

Facultad de Ciencias Naturales y Exactas
Departmento de Física

Degree Thesis

Magnetic properties of spinor boson gases in optical lattices: a Gutzwiller variational approach

by Gustavo MARÍN

We study the magnetic properties of repulsively interacting spin-1 bosons in optical lattices at unit filling in the relevant case of a balanced mixture. Previously, it has been shown that in presence of an external quadratic Zeeman field a rich phase diagram is induced providing both ferromagnetic and antiferromagnetic phases when either the zero-projection dominates or the $\pm$ 1-projections dominate. Moreover, several of these field-induced phases and phase transitions are precluded in traditional spin-1/2 systems, making these spin-1 lattice bosons an ideal play ground to analyze novel quantum magnetism. In the present work by means of an imaginary time-evolution using the variational Gutzwiller ansatz wavefunction, we perform quasi mean-field calculations and obtain the ground state of the system as a function of the interaction strength and the quadratic magnetic field. We put a special attention in the ferromagnetic region of the phase diagram and the transition from the xy-ferro to the Large-D phase.

To characterize the behavior of the system at the different possible phases we make use of a set of observables. Using the energy we determine the criteria to achieve the ground-state for a given external field D, due to quadratic Zeeman effect, and the interaction strength between particles, tuned by the parameter θ. The spin-1 particles allow us to determine three different ferromagnetic phases, the classical Ising-ferro, the xy-ferro and Large-D. Two of them, Ising-ferro and xy-ferro, have a total magnetization different from zero, the first in z-axis or easy-axis and the second in the xy-plane also called easy-plane. The large-D has all the particles in the zero Zeeman level due to the energy gap induced by the external field. These three phases show up in 1D and 2D systems. This method allows us to study qualitatively the field induced phases in the system with ferromagnetic interactions.

We also track down the transition between the xy-ferro and Large-D, using the fidelity susceptibility. This critical field depends on the interaction θ and the dimension of the system. These results are compared with the predicted by the Density Matrix Renormalization Group (DMRG) and the field theory in 1D, and with field theory in 2D. In both 1D and 2D, the results agree astonishing well in the vicinity of the highly symmetric point, $SU(3)$, where the system behaves robustly against perturbations and, hence, the quasi mean-field Gutzwiller reproduces the relevant aspects of the phases and even the precise location of the phase transition. Away from this symmetric point our results diverge from the exact DMRG and field theory results.

Acknowledgements

First and foremost, I have to thank my research supervisor, Prof. Karem Rodríguez. Without their assistance and dedicated involvement in every step throughout the process, this thesis would have never been accomplished.

Contents

List of Figures

Dedicated to my mother and father.

Chapter 1

Introduction

Low dimensional quantum systems show up with a huge variety of new physical phenomena leading to the discovery of new phases and phase transitions. Including the development of new theoretical, experimental and numerical tools to the study of many-body systems. The cooling at extremely cold temperatures (nanokelvins) of atoms, ions, and molecules using techniques such as laser cooling and trapping [1], and evaporative cooling [2], has allowed huge control over the trapped particles [3]. The additional possibility of trapping particles in optical lattices, providing control over parameters and dimensionality of the system, opens a new ideal area to study the phases both theoretically and experimentally [4].

The laser cooling is combined with the evaporative cooling allowing the experimental observation of the Bose-Einstein condensation (BEC) in 1995 [5, 6], a phenomenon predicted by Bose and Einstein between the 1924 [7] and 1925 [8], hence awarding with the Nobel prize of physics in 2001 to a E. Cornell, C. Wieman and W. Ketterle. The physics of ultracold atoms entered the area of the strongly correlated systems with the seminal proposal of D. Jaksch [9], on how to achieve the transition from superfluid to Mott insulator (SF-MI) in optical lattices with cold atoms, the experimental achievement of the transition (SF-MI) by the Bloch-Hänsch group [10] was without doubt the benchmark for further studies [11]. The possibility to change the collision properties, by means of the syntonization of Feshbach resonances [12], allows the experimental realization of systems of the solid state physics, until now unavailable. While the Bose-Hubbard in the condensed matter field is very restricted, the ultracold particles loaded in optical lattices enable the perfect realization of a huge variety of these models [13]. The spin interactions between particle in nearest-neighboring sites could be implemented joining two atoms in one site and carry out controlled collisions [14, 15]. On-site exchange interaction [16], and super exchange interactions [17] have been also achieved. All these systems can be used as quantum simulators of several condensed matter models.

The possibility to trap atoms in a purely optical way opens the prospect to study spinor condensates, which are gases composed by particles with many available Zeeman levels. They constitute an ideal playground to study the interrelation between the external and internal degrees of freedom (spin). As a result the physics of the ground state of the spinor gases is very rich, providing new scenarios for the quantum magnetism [18, 19].

1.1 Bose-Hubbard model

The Hamiltonian that describes a spinless bosonic system loaded in a periodic potential, in the first quantization formalism, is the following

$$\hat{H} = \sum_{\alpha=1}^{N} \left(-\frac{\hbar^2 \boldsymbol{\nabla}_\alpha^2}{2m} + \hat{V}_{ext}(\boldsymbol{r}_\alpha) + \sum_{\beta \neq \alpha}^{N} \hat{V}_{int}(\boldsymbol{r}_\alpha - \boldsymbol{r}_\beta) \right), \tag{1.1}$$

where N is total number of particles, m the mass, $\hat{V}_{ext}(\boldsymbol{r})$ is the external periodic trapping potential and $\hat{V}_{int}(\boldsymbol{r} - \boldsymbol{r}')$ is the interaction potential. In an ultracold system, we only consider binary collisions in the lowest energy orbital, the s-wave, at this limit we obtain an effective scattering length a, which determines the interaction strength. In the Born approximation it is considered the interaction as an effective contact potential, such that,

$$\hat{V}_{int}(\boldsymbol{r} - \boldsymbol{r}') = \frac{4\pi\hbar a}{m} \delta(\boldsymbol{r} - \boldsymbol{r}'). \tag{1.2}$$

The Born approximation works for low density gases, such as the BEC. Going to the second quantization formalism the dynamics of an ultracold diluted Bose gas, in the tight binding region, are described by the Bose-Hubbard (BH) Hamiltonian [9]. In order to keep the system in the tight binding approximation, we assume the energies involved in the system dynamics to be small compared to the excitation energies of the second band, then the on-site interaction energy must be smaller than the excitation energy, i.e. the next band. The BH Hamiltonian, in the grand canonical ensemble, is:

$$\hat{H}_{BH} = -t \sum_{\langle ij \rangle} \left(\hat{b}_i^\dagger \hat{b}_j + h.c. \right) + \frac{U}{2} \sum_i \hat{n}_i \left(\hat{n}_i - 1 \right) - \mu \sum_i \hat{n}_i, \tag{1.3}$$

where $\hat{b}_i (\hat{b}_i^\dagger)$ annihilates (creates) a particle in the i-th site and $\hat{n}_i = \hat{b}_i^\dagger \hat{b}_i$ is the occupation number operator, the first term is the hopping energy, related with the probability of tunneling between nearest-neighboring sites given by t. The second term is the on-site interaction energy whose strength is given by U and the last term is the chemical potential term μ. At zero temperature the system shows a continuous quantum phase transition, this transition is induced by quantum fluctuations in the ground state of the many-body system, when the strength ratio between the two competing energy terms, t/U, is varied across a critical value and it is given a change in the macroscopic properties of the ground state is observed. The strength of the hopping energy, t, is considered to be equal for all sites in the optical lattice and it is given by,

$$t = \int d\boldsymbol{r} \quad \omega_i^*(\boldsymbol{r}) \left(-\frac{\hbar^2 \nabla_\alpha^2}{2m} + \hat{V}_{ext}(\boldsymbol{r}) \right) \omega_j(\boldsymbol{r}), \tag{1.4}$$

where $\omega_j(\boldsymbol{r})$ is the wannier function for a particle located in the j-th site. The strength of the interaction energy, is given by

$$U = \frac{4\pi\hbar a}{m} \int d\boldsymbol{r} \quad |\omega_i(\boldsymbol{r})|^4. \tag{1.5}$$

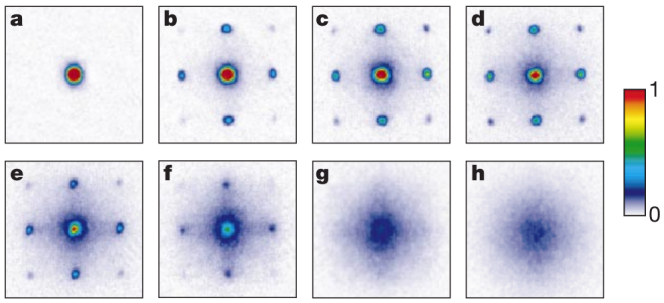

FIGURE 1.1: Absorption images of multiple matter wave interference patterns. These were obtained after suddenly releasing the atoms from an optical lattice potential with different potential depths after a time of flight of 15 ms. Showing the phase transition, in momentum space, from the superfluid at ***a*** in wich the interference pattern shows a highly coherent phase, to the Mott insulator at ***g*** where the phase coherence is lost.

The BH model presents two phases, the Superfluid (SF) and the Mott Insulator (MI), in the first one the kinetic energy is the dominant term, that is $t >> U$, such that all atoms occupy the identically extended Bloch state, meaning the momentum of the system is well-defined. This state is well described by a Poissonian distribution such as coherent states, in this phase we have a long range coherence throughout the lattice. In general for the ground state of a system with N particles and L lattice sites, in the SF phase, we have:

$$|\Psi_{SF}\rangle \propto \left(\sum_{i}^{L} \hat{a}_i^\dagger\right)^N |0\rangle. \tag{1.6}$$

On the other hand, if the on-site interaction is the dominant energy, that is $t << U$, we have that the occupation number of particles per site is fixed to an integer, such that we have the same number of particles, n, at each site, this is the Mott insulator phase. An essential feature of the MI is the existence of a gap in the excitation spectrum, in general the ground state can be written as the tensorial product of Fock states at each lattice site,

$$|\Psi_{MI}\rangle \propto \bigotimes_{i}^{L} \left(\hat{a}_i^\dagger\right)^n |0\rangle. \tag{1.7}$$

This phase transition was first studied theoretically by Fisher at. al.[20], and achieve experimentally by Greiner et. al.[10], showing the continuous and reversible quantum phase transition, see Figure 1.1, from SF to MI, controlling U and t by the periodic lattice depth, manipulating the laser intensity.

1.1.1 Gutzwiller ansatz

Following equations (1.6) and (1.7), the system state can be approximated by the Gutzwiller ansatz [21, 22]. This is a mean field approach where the wave function of the whole system takes the form of a tensorial product between the states of each site in the lattice.

The possible states at each site are local superposition of the occupation states or Fock states,

$$|\Psi\rangle = \bigotimes_i \sum_{n_i=0}^{n_{max}} f_{n_i}^{(i)} |n_i\rangle, \tag{1.8}$$

where n_{max} is the maximum number of allowed particles per site and $f_{n_i}^{(i)}$ are the probability amplitude per site whose sum should hold the normalization condition $\sum_n |f_n^{(i)}| = 1$, for each site i and local state. Here, we have not taken into account the spin degree of freedom, all this description apply for spinless systems. In chapter 2, we have a look in detail at the Gutzwiller approach for spin-1 systems. The ground state amplitudes are achieved by using a variational method which leads the whole system to converge to the ground state energy by means of the minimization of the amplitudes per site. The state of minimum energy is obtained using the time-dependent Schrödinger equation and evolving the Gutzwiller variational wave function in imaginary time [23], as it is described below.

1.2 Spin-1 Bose-Hubbard model

The spin-1 bosonic system is the lowest quantum spin system to exhibit exchange collisions and sensitivity to the quadratic Zeeman effect (QZE), the later plays a crucial role in spin gases with vanishing magnetization and should be take into account for higher spin systems. Despite the experimental relevance the quadratic Zeeman is rarely considered in the literature. The role of an external magnetic field is to enhance the magnetic properties of the spinor bosons.

In this work, we study a system integrated by spin-1 bosonic atoms in a periodic potential under the influence of an external magnetic field and repulsive interactions [24]. In particular, we study the system phases as function of the interactions, paying special attention in the ferromagnetic case. The experimental realization of the model addressed in our work could be feasible in the near future due the unprecedented control gained for the ultracold and diluted gases loaded in optical lattices, such as the previously discussed MI-SF transition already achieved experimentally [10]. Furthermore, considering an optical trapping far from the resonance it is possible the simultaneous trapping of the different Zeeman levels [25, 26].

Strongly interacting spinors loaded in optical lattices show ferromagnetic phases (FM) besides of anti-ferromagnetic (AFM) ones. Varying the intensity of the external field the system undergoes different quantum phases [9]. Among the first ones we could find a FM polar phase where the null spin projection ($m_F = 0$) dominates. On the other hand, when the projections $m_F = \pm 1$ take over the system, the system undergoes either Ising (FM) or the XY-FM [27] phases in the ferro side or in an AFM-XY nematic phase [28]. When the system is in a superposition of all internal projection, it stands in an AFM dimerized phase [29].

To build the spin-1 Bose-Hubbard Hamiltonian, we start from the equation (1.1), but now we have two possible interaction channels, when the total spin of the two interacting particles is $F = 0$ and $F = 2$, the channel $F = 1$ is forbidden due to symmetry considerations of the wave function [30], then the interaction potential is written as

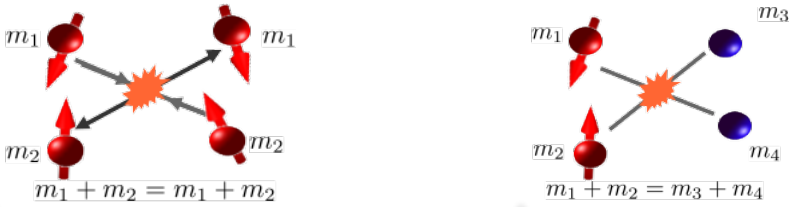

(A) Spin preserving collision.

(B) Spin changing collision.

FIGURE 1.2: Spin-Spin interaction schemes, **(A)**, for spin preserving and **(B)** spin changing collisions, in both cases the total spin projection should be preserved.

$$\hat{V}_{int}(\boldsymbol{r}-\boldsymbol{r}') = \frac{4\pi\hbar}{m}\left(a_0\hat{P}_0 + a_2\hat{P}_2\right)\delta(\boldsymbol{r}-\boldsymbol{r}'), \tag{1.9}$$

where a_F and $\hat{P}_F$ are the scattering length and the projector operator in the channel F, respectively. In the second quantization formalism the Hamiltonian which describes this system is of the Hubbard type, when the system is restricted to the lowest energy band, the process is presented in Appendix A, for spin-1 particles, it is given by [31],

$$\begin{aligned}\hat{H} = -t\sum_{m,\langle ij\rangle}\left(\hat{b}^\dagger_{mi}\hat{b}_{mj} + \hat{b}^\dagger_{mj}\hat{b}_{mi}\right) - \mu\sum_{m,i}\hat{n}_{mi} + Q\sum_{m,i}m^2\hat{n}_{mi} \\ + \sum_i\left\{\frac{g_0+2g_2}{6}\hat{b}^\dagger_{0i}\hat{b}^\dagger_{0i}\hat{b}_{0i}\hat{b}_{0i} + \frac{g_2}{2}\left(\hat{b}^\dagger_{1i}\hat{b}^\dagger_{1i}\hat{b}_{1i}\hat{b}_{1i} + \hat{b}^\dagger_{-1i}\hat{b}^\dagger_{-1i}\hat{b}_{-1i}\hat{b}_{-1i}\right)\right. \\ + \frac{2g_0+g_2}{3}\hat{b}^\dagger_{1i}\hat{b}^\dagger_{-1i}\hat{b}_{-1i}\hat{b}_{1i} + g_2\left(\hat{b}^\dagger_{0i}\hat{b}^\dagger_{-1i}\hat{b}_{-1i}\hat{b}_{0i} + \hat{b}^\dagger_{0i}\hat{b}^\dagger_{1i}\hat{b}_{1i}\hat{b}_{0i}\right) \\ \left. + \frac{g_2-g_0}{3}\left(\hat{b}^\dagger_{0i}\hat{b}^\dagger_{0i}\hat{b}_{-1i}\hat{b}_{1i} + \hat{b}^\dagger_{1i}\hat{b}^\dagger_{-1i}\hat{b}_{0i}\hat{b}_{0i}\right)\right\}.\end{aligned} \tag{1.10}$$

As mentioned above the first term corresponds to the hopping energy between nearest-neighbor lattice sites, the second term represents the chemical potential, the third term shows the quadratic Zeeman field coupling (QZE). The last term is related with the spin-spin interactions between two particles in the same site. Here, the interaction strengths are defined by the scattering length at each channel

$$g_F = \frac{4\pi\hbar a_F}{m}\int d\boldsymbol{r}\quad |\omega_i|^4, \qquad Q = q\int d\boldsymbol{r}\quad |\omega_i|^2. \tag{1.11}$$

In the Hamiltonian (1.10), the last summation describes the interaction, or collision, between two particles. The interaction processes are schematized in the Figure 1.2. We have two different collision behaviors, the first one when the magnetic spin projection of the incoming particles is the same of the outgoing particles after the collision, this process is called spin preserving collision, it is depicted in the Figure 1.2a. On the other hand, when the spin magnetic projection of the involved particles changes after the collision, the process is called spin changing collision, see Figure 1.2b. In both cases the total spin magnetic projection is preserved.

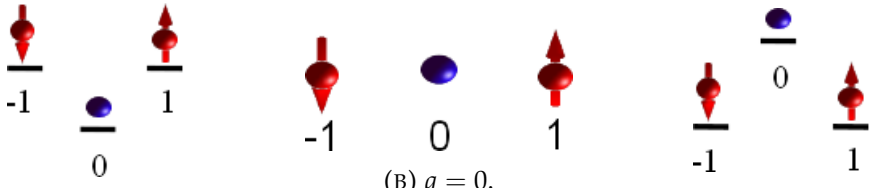

(A) $q > 0$. (B) $q = 0$. (C) $q < 0$.

FIGURE 1.3: Quadratic Zeeman effect scheme. When $q > 0$ $m = 0$ projection is favored whereas for $q < 0$ $m = \pm 1$ projections dominates, $q = 0$ does not leave the degenerancy. This field does not make a difference between the projections $m = -1$ and $m = 1$.

We are looking for field-induced phases in the system, the quadratic magnetic field shifts the Zeeman levels, the schematic representation is shown in Figure 1.3. We have that the $m = \pm 1$ magnetic projections are favored if $q > 0$ (1.3a), the zero projection $(m = 0)$ is favored when $q < 0$ (1.3c). The coefficient q of the QZE could be contributed from an external field (q_B) from a microwave or a light field(q_{MW}): $q = q_B + q_{MW}$, the external field is calculated by using second order perturbation theory [32] as,

$$q_B = \frac{(g\mu_B B)^2}{\Delta E_{hf}}, \tag{1.12}$$

where g is the Landé hyperfine factor, μ_B the Bohr magneton, B the magnetic external field and $\Delta E_{hf} = E_m - E_i$ is the hyperfine energy splitting and it is given by the difference between the initial (E_i) and the intermediate (E_m) energy, the QZE is known in condensed matter field as the single-ion anisotropy effect.

Let us consider that the system is located in the strongly correlated phase of the Mott insulator with only one particle per site where the hopping term behaves as perturbative. We study the behavior of the system under the effect of an external quadratic field, aiming to characterize the magnetic phases, in particular the ferromagnetic phases of the system induced by the external field [31] by means of the Gutzwiller method.

1.3 Effective Hamiltonian in the Mott-insulator regime

Studying the particular case of having just one particle per site in the Mott insulator phase, we build an effective Hamiltonian out of the Bose-Hubbbard Hamiltonian which highlights the main low-lying energy contributions. Using second order quasi-degenerate perturbation theory [33, 34], with the hopping term as the perturbation, we transform our original non-diagonal Hamiltonian to a block type Hamiltonian.

The creation operator $\hat{b}^\dagger_{m,i}$ presented in equation (1.10), creates a particle with spin projection m in the i-th site,

$$\frac{\left(\hat{b}^\dagger_{m,i}\right)^n}{\sqrt{n!}}|\emptyset\rangle = |S, m, n\rangle_i, \tag{1.13}$$

where n is the number of particles in the i-th site with magnetic projection m, and $|\emptyset\rangle$ is the vacuum state. The annihilation and creation operators work as,

$$\hat{b}_{m,i}|S,m,n\rangle_i = \sqrt{n}|S,m,n-1\rangle_i,$$
$$\hat{b}^{\dagger}_{m,i}|S,m,n\rangle_i = \sqrt{n+1}|S,m,n+1\rangle_i,$$

Let us recall the angular momentum operator algebra, the set of $SU(3)$ generators, $\hat{\boldsymbol{S}} = (\hat{S}_x, \hat{S}_y, \hat{S}_z)$ satisfy the commutation relation,

$$[\hat{S}_a, \hat{S}_b] = i\hbar\epsilon_{abc}\hat{S}_c, \tag{1.14}$$

where ϵ_{abc} is the Levi-Civita tensor, $\hat{S}_a$ is the a-th cartesian component, and $\hbar$ is Planck's constant henceforth settle to 1. The set of compatible operators $\left\{\hat{S}_z^{(i)}, \left(\hat{\boldsymbol{S}}^{(i)}\right)^2\right\}$, determine the states such that

$$\hat{S}_z^{(i)}|S=1,m,n\rangle_i = m|S=1,m,n\rangle_i,$$
$$\left(\hat{\boldsymbol{S}}^{(i)}\right)^2|S=1,m,n\rangle_i = S(S+1)|S=1,m,n\rangle_i,$$

$|S=1,m,n\rangle_i$, is the spin state of one particle in the i-th site. Because we only have spin-1 particles we use the shorthand form $|S=1,m,n\rangle_i = |m,n\rangle_i$. Henceforth, we use the state $|n_{-1},n_0,n_1\rangle$, where n_m is the occupation number of the m Zeeman level. So, we build the state using the tensor product and the notation is given by

$$|-1,n_{-1}\rangle_i \otimes |0,n_0\rangle_i \otimes |1,n_1\rangle_i = |n_{-1},n_0,n_1\rangle_i. \tag{1.15}$$

Having only one spin-1 particle per well the possible states, at each well, are shown in the Table 1.1. Having two wells each one filled with only one particle the possible states are given by the tensorial product between the Hilbert's space of each well, this is

$$|n_{-1},n_0,n_1\rangle_1 \bigotimes |n_{-1},n_0,n_1\rangle_2, \qquad n_{-1}+n_0+n_1 = 1, \qquad n_m \in \mathbb{N}. \tag{1.16}$$

TABLE 1.1: System basis having one particle per site.

$\lvert n_{-1},n_0,n_1\rangle$	$Energy(E_0)$
$\lvert 1,0,0\rangle$	$-\mu+Q$
$\lvert 0,1,0\rangle$	$-\mu$
$\lvert 0,0,1\rangle$	$-\mu+Q$

Due to the effect of the hopping term in the Hamiltonian, it is possible for a particle to move to the nearest site, in the case of having two particles in the same well, the spin-changing terms makes non diagonal the local Hamiltonian, as shown in the submatrix (1.17), hence the estates $|1,0,1\rangle$ and $|0,2,0\rangle$ are not part of the eigen-basis,

$$\begin{array}{c} \\ \langle 1,0,1| \\ \langle 0,2,0| \end{array} \begin{array}{c} \begin{array}{cc} |1,0,1\rangle & |0,2,0\rangle \end{array} \\ \begin{pmatrix} 2Q+\frac{2g_0+g_2}{3} & \sqrt{2}\frac{g_2-g_0}{3} \\ \sqrt{2}\frac{g_2-g_0}{3} & \frac{g_0+2g_2}{3} \end{pmatrix} \end{array}. \tag{1.17}$$

TABLE 1.2: Basis having two particles in one site

$\|n_{-1}, n_0, n_1\rangle$	E_0
$\|1,1,0\rangle$	$Q + g_2 - 2\mu$
$\|0,1,1\rangle$	$Q + g_2 - 2\mu$
$\|2,0,0\rangle$	$2Q + g_2 - 2\mu$
$\|0,0,2\rangle$	$2Q + g_2 - 2\mu$
$\|+\rangle$	$\lambda_+ - 2\mu$
$\|-\rangle$	$\lambda_- - 2\mu$

The diagonal terms are shown in the Table 1.2, i.e the spin preserving ones. After the diagonalization of (1.17) the resulting eigen-states are shown in Table 1.3, the corresponding eigen-energies are the following

$$\lambda_\pm = Q + \frac{g_2 + g_0}{2} \pm \frac{1}{2}\sqrt{(g_2 - g_0)^2 + \frac{4}{3}(g_2 - g_0)\,Q + 4Q^2}, \tag{1.18}$$

with

$$\tan\phi = \frac{\lambda_+ - 2Q - \frac{2g_0+g_2}{3}}{\sqrt{2}\frac{g_2-g_0}{3}}. \tag{1.19}$$

At this point the local Hamiltonian is completely diagonal, and we can apply a quasi-degenerate second order perturbation theory via the van-Vleck method [35], to build a matrix representation of the effective Hamiltonian,

$$H^{(2)}_{mm'} = \frac{1}{2}\sum_\gamma \langle m|\hat{H}_t|\gamma\rangle\langle\gamma|\hat{H}_t|m'\rangle \left[\frac{1}{E^0_m - E^0_\gamma} + \frac{1}{E^0_{m'} - E^0_\gamma}\right], \tag{1.20}$$

where $|m\rangle$ and $|m'\rangle$ are the target states considering two particles in two neighboring sites and only one particle per site, i.e, eigen-states listed in the Table 1.1, and the $|\gamma\rangle$ goes over the virtual states with two particles on a single site and an empty site, the states listed in Table 1.2, the term E^0_i is the corresponding energy. The retrieved matrix of this process is:

TABLE 1.3: Eigen-states of matrix (1.17), and its correspondent eigen-energy

Eigenstates	Energy
$\|+\rangle = \cos\phi\|1,0,1\rangle + \sin\phi\|0,2,0\rangle$	λ_+
$\|-\rangle = -\sin\phi\|1,0,1\rangle + \cos\phi\|0,2,0\rangle$	λ_-

$$H^{(2)} = \begin{pmatrix} -\frac{4t^2}{g_2} & 0 & 0 & 0 & 0 & 0 & 0 & 0 & 0 \\ 0 & -\frac{2t^2}{g_2} & 0 & -\frac{2t^2}{g_2} & 0 & 0 & 0 & 0 & 0 \\ 0 & 0 & 2t^2\Delta & 0 & \sqrt{2}t^2\xi & 0 & 2t^2\Delta & 0 & 0 \\ 0 & -\frac{2t^2}{g_2} & 0 & -\frac{2t^2}{g_2} & 0 & 0 & 0 & 0 & 0 \\ 0 & 0 & \sqrt{2}t^2\xi & 0 & -4t^2\Omega & 0 & \sqrt{2}t^2\xi & 0 & 0 \\ 0 & 0 & 0 & 0 & 0 & -\frac{2t^2}{g_2} & 0 & -\frac{2t^2}{g_2} & 0 \\ 0 & 0 & 2t^2\Delta & 0 & \sqrt{2}t^2\xi & 0 & 2t^2\Delta & 0 & 0 \\ 0 & 0 & 0 & 0 & 0 & -\frac{2t^2}{g_2} & 0 & -\frac{2t^2}{g_2} & 0 \\ 0 & 0 & 0 & 0 & 0 & 0 & 0 & 0 & -\frac{4t^2}{g_2} \end{pmatrix}. \quad (1.21)$$

Such that the parameters are given by

$$\Delta = \left(\frac{\cos^2\phi}{2Q-\lambda_+} + \frac{\sin^2\phi}{2Q-\lambda_-}\right),$$
$$\Omega = \left(\frac{\sin^2\phi}{\lambda_+} + \frac{\cos^2\phi}{\lambda_-}\right),$$
$$\xi = \sin\phi\cos\phi\left(\frac{1}{2Q-\lambda_+} - \frac{1}{\lambda_+} - \frac{1}{2Q-\lambda_-} + \frac{1}{\lambda_-}\right).$$

The effective Hamiltonian matrix of eq (1.21) can be written in terms of the spin-1 operators, see Appendix B, as a generalized bilinear-biquadratic Heisenberg (BBH) Hamiltonian as follows,

$$\hat{H} = J\left[\sum_{\langle ij\rangle}\cos\theta\hat{\mathbf{S}}_i\cdot\hat{\mathbf{S}}_j + \sum_{\langle ij\rangle}\sin\theta\left(\hat{\mathbf{S}}_i\cdot\hat{\mathbf{S}}_j\right)^2\right] - DJ\sum_i\left(\hat{S}_i^z\right)^2 \quad (1.22)$$

where $\hat{\vec{S}}_i$ are the spin operators in the i-th site, the sum goes over the nearest-neighboring sites. A standard parametrization has been introduced [29, 31] for the bilinear and biquadratic terms where J is the energy unity defined in the Appendix B, The interaction strength is parameterized by the variable θ. The last term correspond to the quadratic Zeeman field.

1.3.1 Phases in the bilinear-biquadratic Heisenberg model

Without any external field the bilinear-biquadratic Heisenberg model, has a well known ground state phase diagram as a function of the interaction strength θ, for the 1D diagram see figure (1.4). Due to the exchange interaction, the bilinear part in the Hamiltonian, the model exhibits ferromagnetic (FM) [36] and antiferromagnetic (AFM) phases [37], in particular for the $\theta = -\pi$ and $\theta = 0$ points we have the simple Heisenberg model for FM and AFM interactions, we focus our work in the ferromagnetic region and look for the field-induced phases by the QZE.

The ferromagnetic region has a degenerate ground state such that the total spin sum is maximized, for a system with N spin-1 particles $S_{tot} = N$, the FM ground states are

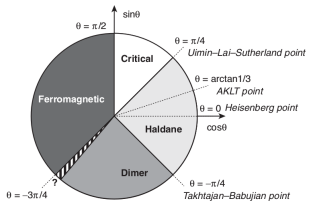

FIGURE 1.4: The complete phase diagram of the bilinear-biquadratic Heisenberg hamiltonian. The present work focuses mainly on the ferromagnetic phase.

not invariant under $SU(2)$ symmetries, for these states $\langle \hat{\boldsymbol{S}} \rangle \neq 0$ such that the system distinguish a certain direction [38].

1.4 Problem statement

We consider a square optical lattice, allowing just one spin-1 boson per site, with repulsive interactions, that is the system is found in the MI regime. Additionally, a quadratic external Zeeman effect is introduced, which includes magnetic phases in the system. To study these phases in the strongly correlated regime, it is necessary to pay attention to the virtual processes of the particles when moving from one well to another, for which the hopping energy is treated in a perturvative way. Hence, we model the system by means of a generalized Heisenberg Hamiltonian, that is, including the spin-spin interactions between neighboring sites. We propose the Gutzwiller ansatz to study the magnetic phases in a quasi-meanfield approach as function of the quadratic external field and the parameterized interaction parameter as it is discussed in Chapter 2. We pay special attention at the regime of the ferromagnetic phases. Several observables are studied in order to characterize the phases and to locate the different phase transtions, the retrieved results are presnted in Chapter 3. Finally, Chapter 4 is devoted to conclusions and perspectives of the present work.

Chapter 2

Gutzwiller variational approach

The Gutzwiller variational many-body wave-function has been an important tool in the study of various quantum correleated systems, it describes particles on a rigid lattice, first proposed by M. C. Gutzwiller [39] for the study of ferromagnetism in transition-metals. It has been widely used for its simplicity and the Gutzwiller approach (GA) has been extended to different systems, ranging from ferromagnets [39, 40], to ultracold bosonic gases [9, 22, 21], to Bose-Fermi mixtures [41], to superconductors [42, 43]. In this chapter, we show all the necessary tools for applying the Gutzwiller approach to our particular case.

2.1 The Gutzwiller approach

The Gutzwiller approach (GA), aproximates the many-body wave-function as a product states of each i-th site

$$|\Psi\rangle = \bigotimes_i \sum_{n_i=0}^{n_{max}} f_{n_i}^{(i)} |n_i\rangle, \tag{2.1}$$

where $|n_i\rangle$ is the Fock state and $f_{n_i}^{(i)}$ are the probability amplitudes which are normalized to $\sum_n |f_n^{(i)}| = 1$. The later are the variational parameters that must be determined by minimizing the energy, where the parameters are enabled to be time-dependent, $f_n^{(i)} \equiv f_n^{(i)}(t)$. To study the dynamics, we are allowed to build a Lagrangian [44, 45] of the system in the state $|\Psi\rangle$, by doing,

$$\mathcal{L} = \frac{i\hbar}{2}\left(\langle\Psi|\dot{\Psi}\rangle - \langle\dot{\Psi}|\Psi\rangle\right) - \langle\Psi|\hat{H}|\Psi\rangle, \tag{2.2}$$

due to hamilton's principle of stationary action this functional is minimized when satisfying the equation:

$$\frac{d}{dt}\left(\frac{\partial\mathcal{L}}{\partial\dot{f}_n^{*i}}\right) = \frac{\partial\mathcal{L}}{\partial f_n^{*i}}. \tag{2.3}$$

For the specific case of the spin-1 in the MI, with one particle per site, we need to modify the GA in (2.1) to make it work in this limit. The states of our GA must be eigen-states of the local Hamiltonian in (1.22), then we can write down our ansatz as,

$$|\Psi\rangle = \bigotimes_i \sum_{m_i=-1}^{1} f_{m_i}^{(i)} |m_i\rangle, \tag{2.4}$$

where m is the magnetic spin projection, and $f_{m_i}^{(i)}$ tell us the probability to get the particle in the i-th site with magnetic spin projection m. In order to solve the dynamics of our system, we follow the Lagrangian discussed above.

2.1.1 Imaginary time evolution

Our objective is obtain the ground-state of the system for a given set of interaction parameters, to achieve this, we use the imaginary time evolution, performing the following time coordinate change $t = -i\tau$. Let $|\phi\rangle$ be an arbitrary state, we can write it in the Hamiltonian eigen-basis, and then apply the time evolution operator, hence, we obtain

$$\langle\phi|U(t)|\phi\rangle = \langle\phi|e^{-\frac{iHt}{\hbar}}|\phi\rangle = \sum_{k,k'}\delta_{k,k'}e^{-\frac{iE_kt}{\hbar}}\langle\phi|k\rangle\langle k'|\phi\rangle = \sum_k e^{-\beta E_k}|\phi_k|^2, \tag{2.5}$$

where the states $|k\rangle$ are the Hamiltonian eigen-states. Now, under the imaginary time evolution we define $\beta = \tau/\hbar$, such that

$$\langle\phi|U(\tau)|\phi\rangle = \sum_k e^{-\frac{E_k\tau}{\hbar}}|\phi_k|^2 = \sum_k e^{-\beta E_k}|\phi_k|^2, \tag{2.6}$$

with $|\phi_k|$ being the projection of $|\phi\rangle$ over $|k\rangle$. Equation (2.6) is the partition function in the canonical ensemble and the thermal density matrix is given by

$$\rho_{k,k'}(\beta) = e^{-\beta E_k}|\phi_k|^2\delta_{k,k'}, \tag{2.7}$$

where the imaginary time τ behaves as the inverse of the temperature T,

$$\beta = \frac{\tau}{\hbar} \sim \frac{1}{k_bT},$$

therefore when $\beta \to \infty$ one reaches the low temperature limit, the sum in (2.6) is dominated by the ground-state term, this allows us to reach the ground state energy and its distribution. On the other hand the imaginary time evolution operator is a decreasing exponential and it decreases faster for states with higher energy. Furthermore, it is not unitary, such that normalizing at each time step we can obtain the ground state energy after an infinite number of steps. Numerically, we use the equations (2.3), replace $t \to -i\tau$, and solve it using the 4th-order Runge-Kutta method.

2.1.2 The Runge-Kutta method

To solve the set of the differential equations we use the classic 4th-order Runge-Kutta (RK4) method [46], whose total accumulated error is of the order $O(\Delta t^4)$. The method is applied for a given differential equation with established initial conditions, of the form

$$\frac{df}{dt} = G(f,t), \qquad f(0) = f_0. \tag{2.8}$$

Having known the solution at time step l, the $l+1$ can be retrieve by means of

$$f_{l+1} = f_l + \frac{1}{6}h\left(k_1 + 2k_2 + 2k_3 + k_4\right), \tag{2.9}$$

where

$$\begin{cases} k_1 = G(t_l, f_l) \\ k_2 = G(t_l + \frac{1}{2}\Delta t, f_l + \frac{1}{2}k_1\Delta t) \\ k_3 = G(t_l + \frac{1}{2}\Delta t, f_l + \frac{1}{2}k_2\Delta t) \\ k_4 = G(t_l + \Delta t, f_l + k_3\Delta t) \end{cases} . \tag{2.10}$$

The k_i are different increments in the slope of the desire curve, the tangent vector is estimated as the weighted average of these slopes. We do not need the dynamic of the system but the ground state, so we use the imaginary time evolution as explained above, such that,

$$i\frac{df}{d\tau} = G(f, -i\tau), \tag{2.11}$$

since we need to ensure the particle conservation, it is necessary to normalize the whole set of variational parameters $f_{n_i}^{(i)}$ at each $\Delta\tau$ step.

2.1.3 Code implementation

The numerical implementation is done by using the C/C++ language, and a basic scheme is shown in the figure (2.1). We start establishing the initial conditions of the system, those are: the interaction strength between neighboring particles (θ), the strength of the QZE field (D), the number of sites L in the lattice, which is the same number particles, and a normalized initial state $|\Psi(\tau = 0)\rangle = |\Psi_0\rangle$ in the Gutzwiller manifold defined by the set of probability amplitudes $\{f_{n_i}^i(\tau = 0)\}$. The second step is to evolve the system by solving the differential equations retrieved by imposing the minimization condition (2.3), in the imaginary time evolution regime (2.11), using the RK4 method to get the evolved wave-function $|\Psi(\Delta\tau)\rangle$. The latter needs to be normalized to guarantee the probability wave function conservation. As third step, we proceed to check if the system is in the ground state, the convergence condition is that the difference between two consecutive energy of the Gutzwiller state does not change for an enough amount of $\tau = N\Delta\tau$ time steps. In the code we ask for the energy difference of the evolved and the previous wave-function, in order words if $|E(\tau) - E(\tau + \Delta\tau)| < 10^{-7}$ is satisfied for $N \sim 10^5$, we achieved the ground-state, otherwise we keep evolving the system until we reach the convergence condition. Finally once we reach the ground-state distribution, $|\Psi_{GS}\rangle$, we proceed to perform the evaluation of all observables, the discussion of the observables and the corresponding results for the spin-1 system are presented in the Chapter 3.

2.2 Gutzwiller dynamical equations

2.2.1 Gutzwiller approach to spin-less model

In order to obtain the dynamical equations of the Gutzwiller variational method, the first step is to calculate the functional $\mathcal{L}$, defined in the equation (2.2), using the Hamiltonian (1.3) and the GA. We write the set of differential equations fulfilling the minimization procedure(2.3), which describes the dynamic of the system, for a system with N number of particles and L number of lattice sites, the set is given by

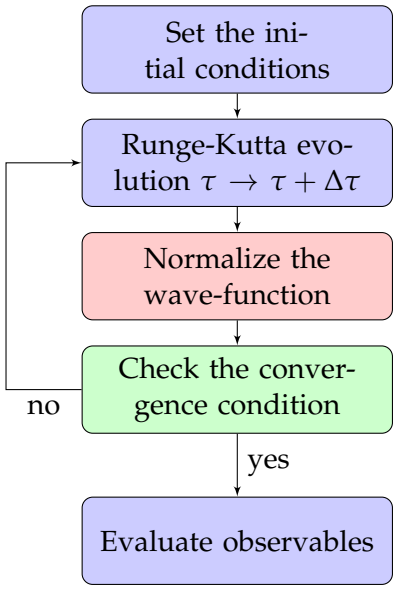

FIGURE 2.1: Basic implementation scheme of the Gutzwiller approach, the imaginary time evolution is used, normalizing at each $\Delta\tau$ step, until the wave-function reaches the convergence, the differential equations are solved by using the RK4 method.

$$
\begin{aligned}
i\hbar\frac{df_n^i}{dt} = -t\sum_m^N \Big[& \sqrt{n(m+1)}f_{n-1}^i \left(f_m^{*i+1} f_{m+1}^{*i+1} + f_m^{*i-1} f_{m+1}^{*i-1} \right) \\
& + \sqrt{m(n+1)}f_{n+1}^i \left(f_m^{*i+1} f_{m+1}^{*i+1} + f_m^{*i-1} f_{m+1}^{*i-1} \right) \Big] \\
& + \frac{U}{2}\sum_m |f_m^i|^2 m(m-1) - \mu \sum_m |f_m^i|^2 m
\end{aligned}
\quad , \tag{2.12}
$$

where i goes over the L lattice sites and $n, m = 0, 1, ..., N$, denote the number of allowed bosons per site, for each Fock state $|n\rangle_i$ in the lattice we have a couple of differential equations, probability amplitudes, f_m^j, of neighboring sites and all the possible occupation number are coupled. The equations are solved, following the scheme in figure (2.1), using Runge-Kutta method and the imaginary time evolution for a given pair of parameters $\{\frac{\mu}{U}, \frac{t}{U}\}$, so we obtain the ground-state $|\Psi(\frac{\mu}{U}, \frac{t}{U})\rangle$. To determine the possible phases of the system we use two observables, the first one is the expected number of particles per site, defined by

$$
\langle \hat{n} \rangle = \sum_i^L \frac{n_i}{L}, \tag{2.13}
$$

where n_i is the expected number of particles in the i-th site. The second observable is the standard deviation of the number of particles, given by,

$$\langle \Delta \hat{n}^2 \rangle = \langle \hat{n}^2 \rangle - \langle \hat{n} \rangle^2 = \sum_i^L \frac{n_i^2}{L} - \left(\sum_i^L \frac{n_i}{L} \right)^2 . \tag{2.14}$$

These two observables have different behaviors in each phase, with these two observables we are able to fully characterize our ground-state function in two distinct phases. At the Mott insulator, all the lattices sites have the same number of particles, we can write down the ground state as,

$$|\Psi_{MI}\rangle = \bigotimes_i^L |n\rangle_i, \tag{2.15}$$

for this regime the expected value of the observables are

$$\langle \hat{n} \rangle_{MI} = n \in \mathbb{N}; \qquad \langle \Delta \hat{n}^2 \rangle_{MI} = 0. \tag{2.16}$$

In the superfluid phase, the state can be written as a Poissonian distribution, such as the coherent states,

$$|\Psi_{SF}\rangle = \bigotimes \left(e^{-\frac{|\alpha_i|^2}{2}} \sum_n \frac{\alpha_i^n}{\sqrt{n_i}} |n\rangle_i \right), \tag{2.17}$$

for the SF state the expected value of the observables are

$$\langle \hat{n} \rangle_{SF} = \sum_i \frac{|\alpha_i|^2}{L} \in \mathbb{R}; \qquad \langle \Delta \hat{n}^2 \rangle_{SF} \neq 0. \tag{2.18}$$

Figure 2.2.A, the results are shown, for the standard deviation $\langle \Delta \hat{n}^2 \rangle$, we can observe the first lobe of the MI, as the black region where $\langle \Delta \hat{n}^2 \rangle = 0$, this phase is surrounded by the SF, with standard deviation different from zero depicted as the color region. In Figure 2.2.B, the results are shown for the expected number of particles, for the first lobe we have $\langle \hat{n} \rangle = 1$, meaning one particle per lattice site, surrounded by SF region in which the expected number of particles varies continuously. We conclude that, using Gutzwiller approach, we were able to establish the phases in the system and the phase transition between them, now we want to use the GA to study the spin-1 system.

2.2.2 Gutzwiller approach to spin-1 BH model

As mentioned above we calculate the functional $\mathcal{L}$, defined in (2.2), but this time using the Hamiltonian (1.22) on the Gutzwiller ansatz (2.4). We obtain $\mathcal{L}$ and the minimization condition (2.3) for a lattice with L sites, with one spin-1 particle per site and magnetic projection m, the final result is:

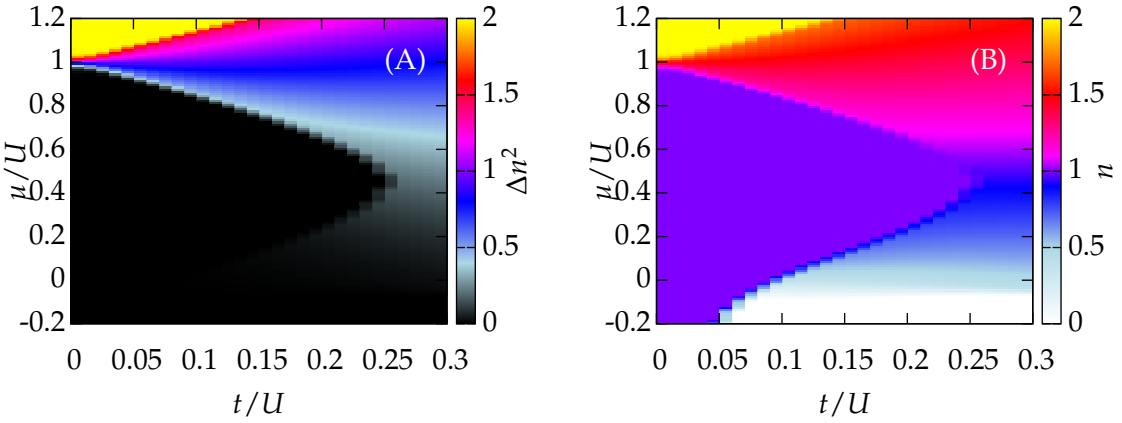

FIGURE 2.2: (A) standart deviation for the number of particles per site as function of the normalized hopping energy t/U and the normalized chemical energy μ/U, in a spinless one dimesional system. (B), expected number of particles per site as function of the normalized hopping energy t/U and the normalized chemical energy μ/U, in a spinless one dimesional system.

$$
\begin{aligned}
i\hbar\frac{df_m^i}{dt} = \frac{1}{2}J\cos\theta\sum_{m'}\Big(&\Omega(m)\Omega(m')f_{m-1}^i f_{m'-1}^{*i+1}f_{m'}^{i+1}\\
&+\Omega(m+1)\Omega(m'+1)f_{m+1}^i f_{m'+1}^{*i+1}f_{m'}^{i+1}+2mm'f_m^i|f_{m'}^{i+1}|^2\Big)\\
&+\frac{1}{4}J\sin\theta\sum_{m'}\Big(\Omega(m)\Omega(m-1)\Omega(m')\Omega(m'-1)f_{m-2}^i f_{m'-2}^{*i+1}f_{m'}^{i+1}\\
&+\Omega(m+1)\Omega(m+2)\Omega(m'+1)\Omega(m'+2)f_{m+1}^i f_{m'+1}^{*i+1}f_{m'}^{i+1}\\
&+\Omega^2(m)\Omega^2(m'+1)f_m^i|f_{m'}^{i+1}|^2+\Omega(m+1)\Omega(m')f_m^i|f_{m'}^{i+1}|^2\\
&+4m^2m'^2f_m^i|f_{m'}^{i+1}|^2+2m\Omega(m)(m'-1)\Omega(m')f_{m-1}^i f_{m'-1}^{*i+1}f_{m'}^{i+1}\\
&+2m\Omega(m-1)(m'+1)\Omega(m'+1)f_{m+1}^i f_{m'+1}^{*i+1}f_{m'}^{i+1}\\
&+2(m-1)\Omega(m)m'\Omega(m')f_{m-1}^i f_{m'-1}^{*i+1}f_{m'}^{i+1}\\
&++2(m+1)\Omega(m+1)m'\Omega(m'+1)f_{m+1}^i f_{m'+1}^{*i+1}f_{m'}^{i+1}\Big)-JDm^2f_m^i
\end{aligned}
\quad , \tag{2.19}
$$

where

$$\Omega(m)=\sqrt{2-m(m-1)}.$$

Equation (2.19) describes the dynamic of the probability amplitude, f_m^i, of the i-th site with magnetic projection m, wich couples with the amplitude at $i+1$. The term accompanied by the $\cos\theta$ function, is related with the bilinear term, in the BBH Hamiltonian (1.22), which coupled nearest Zemann levels, in other words, i.e. it does not

couple $m = 1$ and $m = -1$. The second term, accompanied by the $\sin\theta$ function, is related with the biquadratic term in the BBH Hamiltonian, which coupled all the Zemann levels, the last term is the QZE field. The next step is to use the imaginary time evolution and the RK4 method to find numerically the ground state for a given parameters set and make the proper evaluations. The observables used to characterize the phases are discussed in Chapter 3.

Chapter 3

Spin-1 ferromagnetic phases and phase transitions

With the objective of characterizing the ground state of the system in the thermodynamic limit, we evaluate the expected value of a set of operators for a given pair of parameters in a lattice with periodic boundary conditions. The set of operators is conformed by: chirality $\hat{\tau}$, the spin cartesian components and their square powers, the energy E, and the magnetic susceptibility $\chi(D)$. The expected value of all observables are presented as function of the quadratic external field, D, and the interaction parameter, θ.

3.1 Observables

3.1.1 Energy and density profiles

The ground state energy gives us information about the nature of the analyzed phase transitions following the Ginzburg-Landau point of view. If we have discontinuities in the first derivative we have first order transition, for discontinuities in the second derivative we have second order transition. The value of the energy depends on the value of the interaction strength, θ, and the external field D,

$$E = \langle\psi|\hat{H}|\psi\rangle, \tag{3.1}$$

where $\hat{H}$ is the effective Hamiltonian (1.10), and $|\psi\rangle$ is the retrieve ground-state following the procedure described in subsection (2.2.2). To understand the local behavior we study the probability density profile, which describes the probability to get a particle with m projection in the i-th site, provided by the Gutzwiller probability amplitudes,

$$|f^{(i)}_{m_i}|^2 = \langle\psi|m_i\rangle\langle m_i|\psi\rangle. \tag{3.2}$$

3.1.2 Chirality

This observable distinguishes between phases which are susceptible to the QZE and the non susceptible ones, it is defined as

$$\langle\hat{\tau}^{(i)}\rangle = \langle 3\hat{S}^2_z - 2\rangle_i = |f^i_{-1}|^2 + |f^i_1|^2 - 2|f^i_0|^2. \tag{3.3}$$

For a system with all population in $m = 0$ we get $\tau = -2$, case in which the energy of the system is independent of the external field. When $\tau = 1$, we have all the population distributed in $m = \pm 1$ either in both or one of them, in this case the particles get coupled with the external field D, these constitute the two limiting cases. Otherwise, when there is a coupling among the three magnetic projections, the chirality gets values in the interval $-2 < \tau < 1$. The total chirality τ of the lattice is the average value over the L lattice sites,

$$\tau = \sum_i \frac{\langle \tau^{(i)} \rangle}{L}. \tag{3.4}$$

This operator is one of the $SU(3)$ group generator [28], which describes quadrupolar (nematic) properties.

3.1.3 Fidelity suceptibility

The fidelity, $\mathcal{F}$, is a measurement of similarity between two states, to compare how alike are two states we make the projection of one onto another while slight changes in an external parameter are performed. It is defined as

$$\mathcal{F}(D, \delta D) = |\langle \psi(D) | \psi(D + \delta D) \rangle|, \tag{3.5}$$

when $|\psi(D)\rangle$ and $|\psi(D + \delta D)\rangle$ are two ground states in different quantum phases with different structure properties, the fidelity must be near to zero. At zero temperature the quantum phase transition is driven by the parameters of the Hamiltonian, in the particular case of field-induced phases the QZE is the driving field tuned by the parameter D. For the determination of the phase transition, we study the fidelity susceptibility $\chi(D)$ or, in other words, the response of the fidelity to the driving parameter. For the case of magnetic driven transitions it is also called magnetic susceptibility [47]. It tells us about the behavior of the system under small changes of the external field D, near phase transitions we expect $\chi \neq 0$ and zero otherwise. This is a helpful operator for 1st order, 2nd order transitions and higher order quantum phase transitions,

$$\chi(D) = \lim_{\delta D \to 0} \frac{-2 ln \mathcal{F}(D, D + \delta D)}{\delta D^2}. \tag{3.6}$$

The equation (3.6) behaves controllably sharp and shows the critical parameter value D_c where the transition occurs, hence for two near states at both sides of the critical point we expect a narrow peak, for the fidelity susceptibility.

3.1.4 Spin operators

In order to characterize different magnetic phases, we use the cartesian components of the spin operator, $\hat{S}_x$, $\hat{S}_y$ and $\hat{S}_z$ to establish the magnetic projections of the system, this is the set of the $SU(2)$ generators in an irreducible representation. They satisfy the condition

$$\left[\hat{S}_a^{(i)}, \hat{S}_b^{(j)}\right] = i\delta_{i,j}\epsilon_{abc}\hat{S}_c^{(i)}, \tag{3.7}$$

where $a, b, c = x, y, z$ and the indexes i, j go over the lattice sites. This algebra is similar to the rotation algebra in $\mathbb{R}^3$, the algebra of the $SO(3)$ Lie group. Moreover, the vector $\hat{\mathbf{S}}^{(i)}$ tell us the orientation of the spin, but due to uncertainty principle we cannot measure all three components of the quantum spin simultaneously. The total magnetic projection in the z-axis is determined by the operator $\hat{S}_z$, such that

$$S_z = \sum_i \frac{\langle \hat{S}_z^{(i)} \rangle}{L} = \sum_i \frac{|f_1^i|^2 - |f_{-1}^i|^2}{L}, \tag{3.8}$$

where $f_{m_i}^{(i)}$ is defined in equation (2.19) and L is the number of lattice sites. The magnetic projection in the x-axis perpendicular to the magnetic field axis is given by

$$\langle \hat{S}_x^{(i)} \rangle = \frac{1}{\sqrt{2}} \left(f_{-1}^{i*} f_0^i + f_0^{i*} f_{-1}^i + f_0^{i*} f_1^i + f_1^{i*} f_0^i \right), \tag{3.9}$$

the total x-axis projection S_x is calculated as the total magnetization S_z and the total chirality τ . Second order spin operators are also studied and give us information of the biquadratic part of the BBH Hamiltonian (1.22), the two hermitian operators studied in this work are written in terms of the spin ladder operators, such as,

$$\left\langle \left(\hat{S}_+^{(i)} \right)^2 + \left(\hat{S}_-^{(i)} \right)^2 \right\rangle, \tag{3.10}$$

transitions can be described with this operator, if the particle in the i-th site has either magnetic projection $m = \pm 1$ or superposition of them, if most of the system is in the magnetic projection $m = 0$ this operator has almost no contribution to the expectation value. The second hermitian operator of this kind is of the form

$$\left\langle \hat{S}_+^{(i)} \hat{S}_-^{(i)} + \hat{S}_-^{(i)} \hat{S}_+^{(i)} \right\rangle, \tag{3.11}$$

this operator has always non-vanishing value, nevertheless, its contribution rises if the whole system is in the magnetic projection $m = 0$, the total value of these two operators is the average over all sites in the lattice, as it has been done for the above observables.

3.2 Results for the one dimensional system

Henceforth, the presented results are retrieved by means of the variational method for a one dimensional system using 50 lattice sites and periodic boundary conditions.The discussion about them are presented in this section. Here the BBH hamiltonian (1.22) is normalized to J, which have energy units, such that system becomes dimesionless,

$$\hat{H}_{BBH} \to \frac{\hat{H}_{BBH}}{J}.$$

3.2.1 Convergence and profiles

Using the Gutzwiller approach, and following the implementation scheme presented in Figure 2.1, with the set of equations (2.19) and evolving it in the imaginary time (2.6),

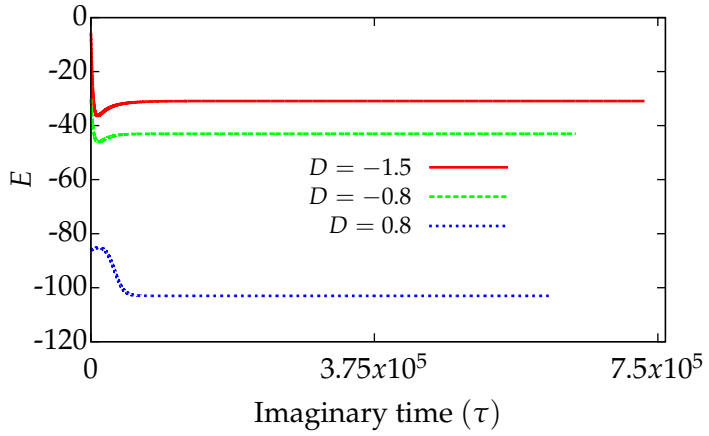

FIGURE 3.1: Convergences for three different QZE external fields, D, for a given interaction strength $\theta = -0.9\pi$, the process is stopped once convergence condition is achieved, here τ is the imaginary time.

the wave function should converge at some finite time $\tau = N\Delta\tau$. After a finite number of iterations, N, the total energy should not vary anymore, in our case the precision is settled to $\Delta E = 10^{-7}$. Figure 3.1 shows the convergence in the imaginary time evolution for the parameters $\{D = -1.5, D = -0.8, D = 0.8\}$ and $\theta = -0.9\pi$. Although in these three example the convergence behaves similarly, it is not always the same, for some parameters the convergence is faster, and the final energy E clearly depends on the parameters. The convergence of the system henceforth is checked for all pair of parameters D and θ.

Once the iterations had converged, we could do all our measurements on the achieved ground-state wave function. In the Figure 3.2 we present the probability density per site for same three cases of the Figure 3.1. First, for $D = -1.5$, we have all particles in the zero Zeeman projection. Second, for $D = -0.8$, we have some population, equally distributed, in the Zeeman levels $m = 1$ and $m = -1$ at each site, but the majority of the population is in $m = 0$, in any case the total magnetization is always zero. Third, for $D = 0.8$, the magnetic projection $m = -1$ overtakes the system, therefore the total magnetization of the system is different from zero. Thus, we have three different behaviors, and we are able to characterize the phases and their boundaries, looking for the critical field values, using the observables presented above.

3.2.2 Ferromagnetic phases

$D > 0$. The first expected phase is the classical *Ising ferromagnet*, this phase has a total magnetization different from zero in the axis of the external field. Figure 3.3 presents S_z as a function of the QZE. We have a spontaneous magnetized ground state for $D > 0$, nematic operators, such as $\hat{S}_z^2$ and $\hat{\tau}$, present a phase dominated by the Zeeman levels $m = \pm 1$, however, these operators do not make any distinction between these two projections. The quadratic Zeeman effect, for $D > 0$, favors the Zeeman levels $m = \pm 1$, as the nematic operators, again without making any distinction between these two projections. The BBH Hamiltonian (1.22) cannot distinguish if a system has all the particles

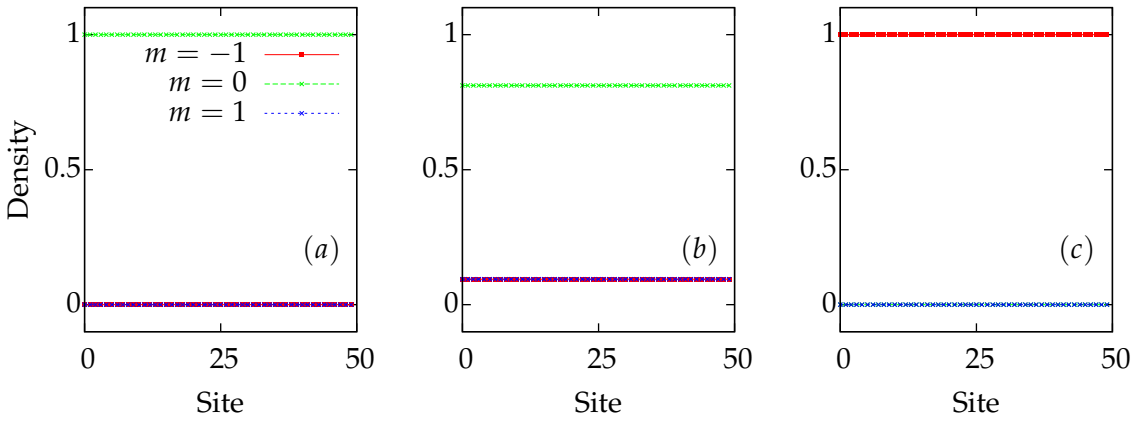

FIGURE 3.2: (a) Density profile per site at the point $\theta = -0.9\pi$ and $D = -1.5$, in this distribution the $m = 0$ projection takes over the system, this is the Large-D unmagnetized phase. (b) Density profile per site at the point $\theta = -0.9\pi$ and $D = -0.8$, the population is ditributed in all Zeeman levels for each particle, $m = 1$ and $m = -1$ have equal probabilities such that the system is unmagnetized but in the xy-Ferro phase. (c) Density profile per site at the point $\theta = -0.9\pi$ and $D = 0.8$, the projection $m = -1$ takes over, the system gets a spontaneous magnetization, this is the Ising-Ferro phase.

parallel or anti parallel to the external field, both configurations have the same energy, meaning that the ground-state has a degenerate Ising-Ferro phase.

$D < D_c < 0$. For $D \ll 0$, the gap between the projections $m = 0$ and $m = \pm 1$ leaves no option to the particles but to stand in the zero magnetic projection, so the BBH Hamiltonian (1.22) has no magnetic response, $S_z = S_x = 0$ and $S_z^2 = 0$, this is the so-called *Large-D* phase. The nematic observable τ, in Figure 3.3, shows that for $D < D_c < 0$ each lattice site is overtaken by the zero Zeeman prejection, where $D_c = D_c(\theta)$ is the critical field between the large-D phase and the xy-ferro phase.

$D_c < D < 0$. The xy ferromagnet has zero total magnetization in the z-axis, $S_z = 0$, but different from zero in the xy-plane. Figure 3.3 also presents a region in which $S_z = 0$ and $S_x \neq 0$, for $D_c < D < 0$. The xy-Ferro phase presents a superposition among all Zeeman levels at each site, as it is show by the nematic operators in Figure 3.3, even though for $D < 0$ the QZE benefits the $m = 0$ projection, the gap is not big enough to cancel $m = \pm 1$ contributions.

At the particular interaction value of $\theta = -0.75\pi$, we are located in a transition line, see Figure 1.4, when $D = 0$ it is also a $SU(3)$ highly symmetric point. The observables show a different behavior from the discussion above, first, the system does not present a xy-ferro phase, it only has two phases with a transition point at $D = 0$, as it is shown by $\chi(D)$ in Figure 3.4. When $D < 0$ the system undergoes the Large-D, but for $D > 0$, the quadratic spin ladder operator, in Figure 3.4, shows us a phase which differs from the Ising-Ferro behavior, where the expected value should be zero.

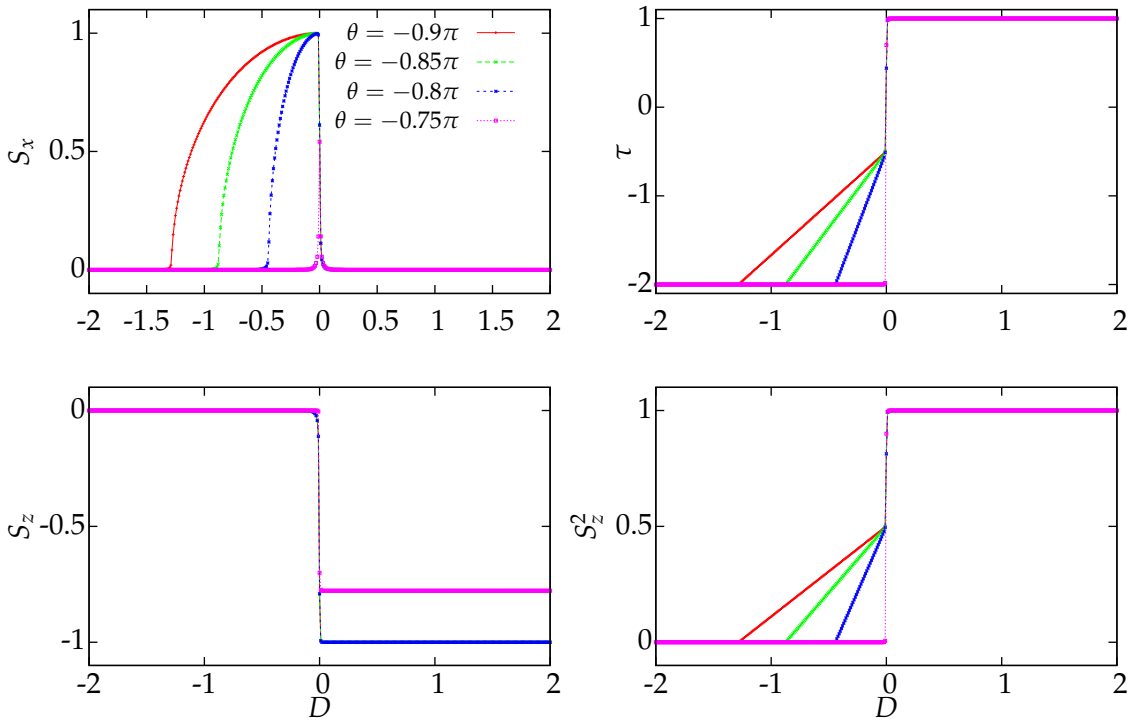

FIGURE 3.3: In a 1D chain. Expected value of $\hat{S}_x$, the system shows magnetic projections along the xy-plane, when undergoes the xy-Ferro. Expected value of $\hat{\tau}$, we observe three different regimes, the Ising-Ferro when $\tau = -2$, Large-D when $\tau = 1$, and xy-Ferro otherwise. Expected value of $\hat{S}_z$, the total magnetization in the z-axis is zero for all the phases at $D < 0$, the magnetized phase, at $D > 0$ is the Ising-Ferro. The expected value of $\hat{S}_z^2$, also shows the three regimes.

If we measure the total energy, E, see Figure 3.4, we observe the dependence of the energy as a function of the external field, $E = E(D)$. For the Large-D the energy is a constant, hence the energy does not have contribution of the QZE field. In the xy-ferro region the energy is linear dependent, the same occurs in the Ising-ferro but the slope change between both phases. The energy in both phases shows a dependence on θ, it shifts downwards as the field is increased. It is important to note that the slope at each phase does not change while varying θ, nevertheless the critical field D_c, the transition point between the Large-D and the xy-ferro, strongly depends on the interaction between particles. The critical field values are track down using the magnetic susceptibility $\chi(D)$, shown in Figure 3.4, we note that the transition points form the xy-ferro to the Ising-Ferro are located in $D = 0$ for all values of θ.

Lattice size. All the previously discussed results were obtained from a 50 lattice sites, given that we are interested in the thermodynamic properties of the system, we make measurements with larger lattices. In Figure 3.5, we show the critical field $D_c(\theta)$, determined by sharp peaks in $\chi(D)$, for $\theta = -0.8\pi$ with different lattice sizes, the critical

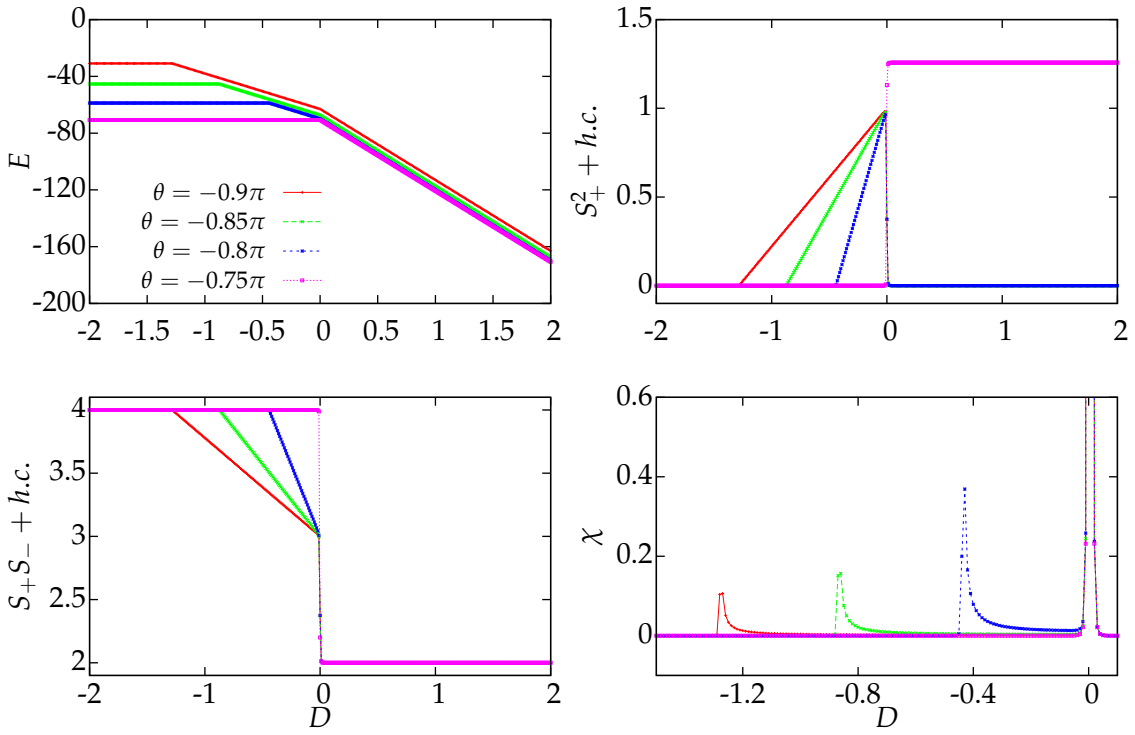

FIGURE 3.4: In a 1D chain. Expected value of $\hat{H}$, the energy dependence on the external field is conditioned to the phases. The quadratic ladder operators shows the three phases, and also confirm that for $\theta = -0.75\pi$, we have a critical point in the Ising-Ferro side. The Magnetic susceptibility $\chi(D)$, shows two critical points, except for $\theta = -0.75\pi$, in which we only have one transition.

field $D_c(\theta)$ does not change significantly, meaning that 50 sites in the lattice are enough to study the system in the thermodynamic limit.

3.2.3 Two dimensional lattice system

Applying the Gutzwiller approach to a two-dimensional lattice, we obtain a new set of differential equations. In the square lattice, we have four nearest sites instead of two like in the one dimensional chain, therefore the equations are similar. The set of dynamic equations of the 2D square lattice are presented in Appendix C. Results for the two-dimensional system are presented in the Figure 3.6, using a square lattice of $10x10$ sites, $L = 100$. This system converges faster than the 1D chain for the same number of sites as expected, because of the mean field nature of the Gutzwiller ansatz. As expected the total magnetization, S_z, presents an spontaneous magnetized phase for $D > 0$, see Figure 3.6, for $D << 0$ the chirality, τ, shows a phase dominated by $m = 0$ and finally the total magnetization in x-axis, S_x, has nonzero values in a region between the large-D and Ising-ferro.

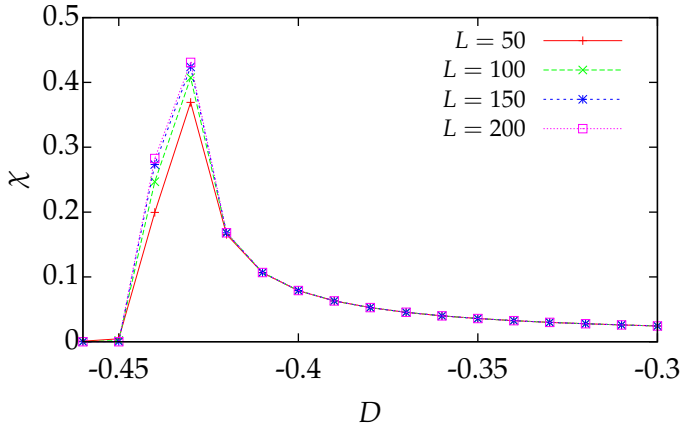

FIGURE 3.5: Here we show the susceptibility $\chi(D)$, for different lattice sizes L for the 1D case. The interaction parameter is set to $\theta = -0.8\pi$.

In summary, the behavior of the phases in 2D is basically the same we had found for the one dimensional lattice, as expected. However, the xy-ferro phase has been enlarged. The transition point between xy-ferro to Ising-ferro stands at zero field for all values of θ, but the transition between Large-D and xy-ferro occurs at the critical point $D_c(\theta)$ for $D < 0$ at larger fields in absolute value than the 1D chain.

3.3 Phase diagram

The full phase diagram, locating the phases and phase transition is presented in the Figure 3.7. The chirality τ, for the 2D lattice, is presented as a function of the parameters θ and D and it is presented as a density plot. The critical field, D_c, is estimated using the susceptibility, $\chi(D)$, which corresponds to the location of the phase transition, the square doted line stands for the 2D lattice whereas the circular dotted line stands for the 1D chain.

The transition line between the xy-ferro and the Large-D, is compared with results obtained by means of the Density Matrix Renormalization Group (DMRG) [31] method and field theory approach for 1D, and for the 2D system with the field theory results, as it is shown in Figure 3.7. The field theory gives us a guess of the phase transition, these curves were taken from Rodriguez *et.al.* [31], in which they include fluctuations for the field theory estimation of the phase transition, in both 1D and 2D. Furthermore, the DMRG gives an exact numerical solution of it. The critical field by means of the GA in 1D, D_c^{1D}, agree with the Field theory and DMRG results near the $SU(3)$ symmetric point, far from $SU(3)$ we have a strong deviation. In one dimension, the quantum fluctuations are relevant for the behavior of any quantum system at low temperatures. Due to its mean-field nature of the Gutzwiller approach (GA) do not have this kind of information. Nevertheless, near the highly symmetric point the system is robust to quantum fluctuations, such that the GA works properly in the vicinity of this point for the spin chain. In 2D, we do not have exact results to compare with, anyway our approach match with the field theory near the $SU(3)$ point.

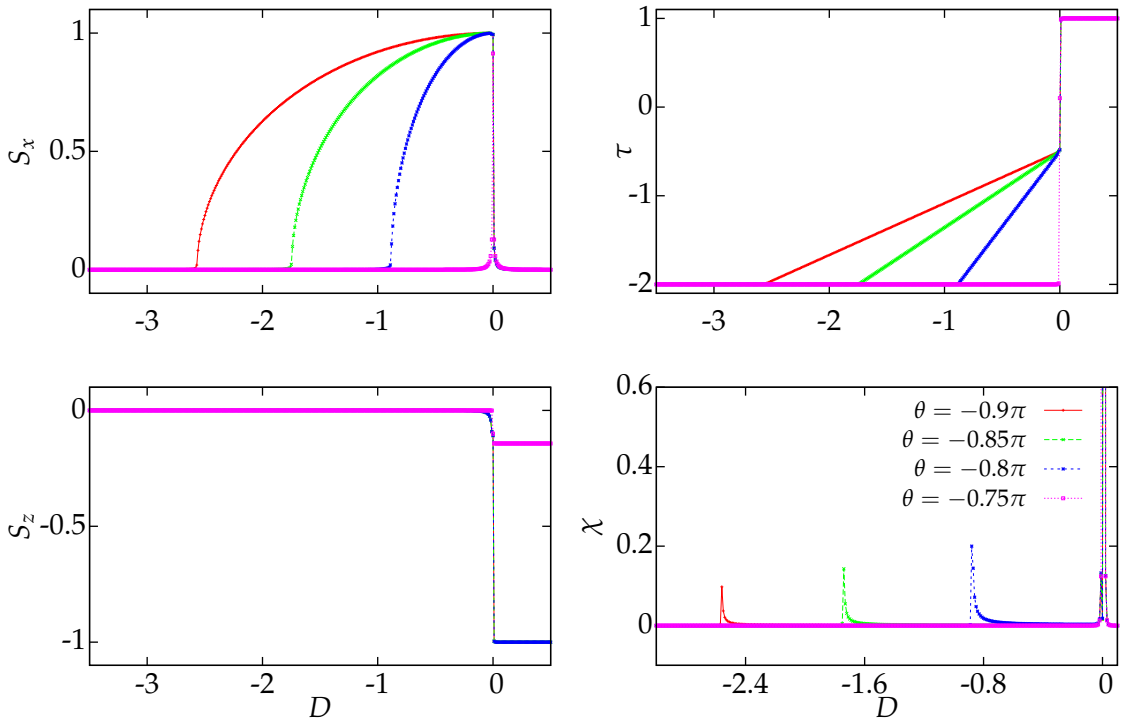

FIGURE 3.6: In a 2D lattice: S_x, the system shows magnetic projection along the x-axis. Expected value of $\hat{\tau}$, we observe three different regimes, the Ising-Ferro when $\tau = -2$, Large-D when $\tau = 1$, and xy-Ferro otherwise. $\hat{S}_z$, the total magnetization in the z-axis is zero for all the phases at $D < 0$, the magnetized phase, at $D > 0$ is the Ising-Ferro. $\chi(D)$, shows two critical points, except for $\theta = -0.75\pi$, in which we only have one transition.

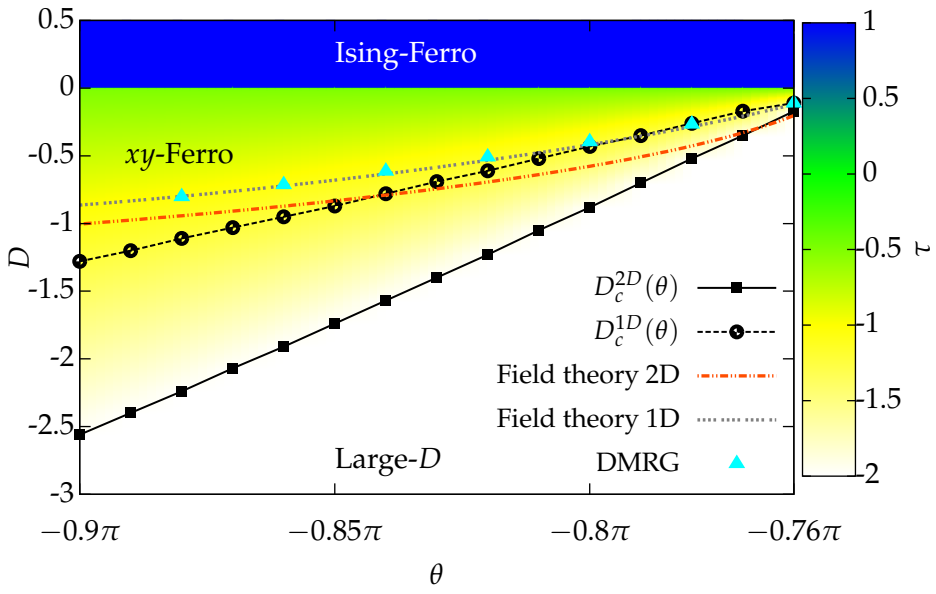

FIGURE 3.7: The density plot display the expected values of the chirality τ for a 2D system as function of the interaction parameter θ and the external field D, In black the transition line $D_c(D,\theta)$ estimated according to fidelity Susceptibility $\chi(D)$ for the 1D system with filled circles ans 2D with filled squares. The full diagram shows the region of each of the three phases of the system. The observables $\chi(D)$ and τ agree in the phase transition, between Large-D and xy-Ferro.

Chapter 4

Conclusions and Perspectives

4.1 Conclusions

In this work, we studied magnetic-induced phases for repulsively interacting spin-1 particles loaded in optical lattices, described by the spin-1 Bose-Hubbard model, the considered external magnetic field induces a quadratic Zeeman coupling with the particles. We work in the particular case of one particle per site being in the first Mott insulator lobe, and then taking the hopping term of the Hamiltonian as a perturbation. We used quasi-degenerate second order perturbation theory, the van-Vleck formalism, to build an effective Hamiltonian for our case of interest. The effective Hamiltonian can be approximated to a bilinear-biquadratic Heisenberg Hamiltonian with ferromagnetic and antiferromagnetic interactions. We were looking for the ground-states properties as function of the external field and the strength interaction focused in the ferro side. Hence, we used the Gutzwiller ansatz as general solution and by means of a variational method build the set of mean field dynamical equations of the system. In order to achieve the system ground-state, we evolve the system in the imaginary time, solving it numerically using the 4-th order Runge-Kutta until the convergence condition is achieved. Finally, we characterize the properties of the ground-state, measuring our observables set.

We are able to characterize three different field induced phases in both a 1D chain and a 2D square lattice. The Ising-ferromagnetic phase in which the ground-state gets spontaneously magnetized in the direction of the field, as effect of the external field which favors the magnetic projections $m = \pm 1$. The second is the xy-ferromagnetic phase, the system also has total magnetization, but this time in the xy-plane, due to interaction between the particles in neighboring sites. The last is the Large-D phase, with lack of magnetization, all particles are located in the $m = 0$ magnetic projection due to the energy gap induced by the external field. These three phases are the expected phases in the ferromagnetic region. Even though our mean-field approach does not involve quantum fluctuations near the $SU(3)$ symmetric point the estimation match with the theoretical predictions of the Field theory and the DMRG calculations. Far from $SU(3)$, the transition between xy-ferro and Large-D is overestimated in our approach.

This approach allows us to test several local observables. The spin operators, including the chirality $\hat{\tau}$, gave us the spin behavior in each phase. The energy observable is crucial for the achievement of the ground-states, since it determines the convergence criterion. Furthermore, the magnetic induced phase transitions are tracked down using the fidelity susceptibility.

Testing the behavior of the system for larger lattices, we are able to conclude that 50 sites are enough to work in the thermodynamic limit. This behavior is expected due to the periodic boundary condition imposed to the system. Our observable set allow us the qualitative description of the phases and location of the phase transitions for 1D and 2D lattices, the full phases diagram is presented in the Figure 3.7 which constitutes a complete summary of the work performed in the present document.

4.2 Perspectives

We expect that for a two-dimensional system the quantum fluctuations to be less relevant, it would be important to compare our current results with the estimation of the field theory without quantum fluctuations.

With the methodology used in the present work, it is possible to qualitatively study the full magnetic induced phase diagram of the bilinear-biquadratic Heisenberg Hamiltonian. It is proposed to go further and look for all possible achievable phases in this Hamiltonian, in other words, extend the use of the Gutzwiller approach to the antiferromagnetic side of the phase diagram in order to analyze the Haldane, critical and dimerized phases under the effect of the quadratic Zeeman effect to establish the availability and limits of this quasi mean-field method. More observables need to be tested in order to characterize all possible phases, like the topological ones.

A disadvantage of the numerical method is the locality of the wave function, which do not allow the study of entangled states neither the calculation of the correlations nor non-local observables. It is possible to improve the Gutzwiller wave-function, using a two site basis, looking for a better approximation of the phase transition between xy-ferro and large-D. A two site basis also can help to get a qualitative approximation to other phases in the BBH such the dimerized one.

Appendix A

Spin-1 Bose-Hubbard Hamiltonian

In this appendix we show that, for spin-1 systems the channel $F = 1$ is a forbidden interaction channel, and show the process to get the spin-1 Bose-Hubbard Hamiltonian from the single particle Hamiltonian.

A.1 Interaction potential

Let us define the spin operators for two interacting particles system, $\{\hat{\boldsymbol{S}}_{(1)}, \hat{\boldsymbol{S}}_{(2)}\}$. These two operators build a new set of operators for the coupled system,

$$\hat{\boldsymbol{F}} = \hat{\boldsymbol{S}}_{(1)} + \hat{\boldsymbol{S}}_{(2)}. \tag{A.1}$$

The new appropriate set of compatible operators to describe the interactions in the coupled system is given by

$$\left\{\hat{\boldsymbol{F}}^2, \hat{S}_z, \left(\hat{\boldsymbol{S}}_{(1)}\right)^2, \left(\hat{\boldsymbol{S}}_{(2)}\right)^2\right\}, \tag{A.2}$$

which defines the set of eigenstates, $\{|S_1, S_2; F, M\rangle\}$, where $|S_{(1)} - S_{(2)}| \leq F \leq S^{(1)} + S^{(2)}$ and $-F \leq M \leq F$. The former in the coupled basis. The uncoupled basis is defined by the set of the states $\{|S_1, m_1; S_2, m_2\rangle\}$. We are allowed to change between these two basis, by means of the Clebsh-Gordan coefficients. Since the total spin F is conserved in a binary collision, the interaction Hamiltonian can be divided according to the spin channel F as

$$\hat{V}(\boldsymbol{r} - \boldsymbol{r}') = \sum_F \hat{V}^F(\boldsymbol{r} - \boldsymbol{r}') = \frac{4\pi\hbar^2}{m} \sum_F a_F \hat{P}_F \delta(\boldsymbol{r} - \boldsymbol{r}'), \tag{A.3}$$

here, m is the reduced mass, a_F is the s-wave effective scattering length and $\hat{P}_F$ is the projector operator in the F channel, the potential is defined as a contact potential. We have considered binary collisions in the lowest orbital level, for each interacting channel. Let us focus in the particular case of spin-1 particles, in which $F = 0, 1, 2$, studying

the behavior in the channel $F = 1$ we get

$$\begin{aligned}\hat{V}^1(\boldsymbol{r}-\boldsymbol{r}') &= g_1\delta(\boldsymbol{r}-\boldsymbol{r}')\hat{P}_1 \\ &= g_1\delta(\boldsymbol{r}-\boldsymbol{r}')\sum_{m,m',n,n'}|1m;1m'\rangle\langle 1m;1m'|\hat{P}_1|1n;1n'\rangle\langle 1n;1n'| \\ &= g_1\delta(\boldsymbol{r}-\boldsymbol{r}')\sum_M\left(\sum_{m,m',n,n'}\langle 1m;1m'|1,M\rangle\langle 1,M|1n;1n'\rangle\right)|1,m;1,m'\rangle\langle 1,n;1,n'|\end{aligned} \tag{A.4}$$

The term in parentheses are the matrix elements of the projector. By simple algebra one can show that

$$\sum_{m,m',n,n'}\langle 1m;1m'|1,M\rangle\langle 1,M|1n;1n'\rangle = 0, \qquad \forall M. \tag{A.5}$$

The projection operator in the channel $F = 1$ is identically to zero, in general it is possible to show that in bosonic systems F must be even to allow interactions [30]. Hence, the interactions between two spin-1 particles only are allowed in the channels $F = 0, 2$, where F is the total spin of both particles. The interaction Hamiltonian can be written down as,

$$\hat{V}(\boldsymbol{r}_1-\boldsymbol{r}_2) = \frac{4\pi\hbar^2}{m}\left(a_0\hat{P}_0 + a_2\hat{P}_2\right)\delta(\boldsymbol{r}_1-\boldsymbol{r}_2). \tag{A.6}$$

For simplicity, we want to re-write the effective potential in terms of the spin operators, we know that $\left(\hat{\boldsymbol{F}}\right)^2 = \left(\hat{\boldsymbol{S}}_1+\hat{\boldsymbol{S}}_2\right)^2$, from which we have the relations [30],

$$\hat{P}_0 + \hat{P}_2 = 1, \qquad \hat{\boldsymbol{S}}_1\cdot\hat{\boldsymbol{S}}_2 = \lambda_0\hat{P}_0 + \lambda_2\hat{P}_2, \tag{A.7}$$

where

$$\begin{aligned}\hat{\boldsymbol{S}}_1\cdot\hat{\boldsymbol{S}}_2|0M\rangle &= -2|0M\rangle = \lambda_0|0M\rangle, \\ \hat{\boldsymbol{S}}_1\cdot\hat{\boldsymbol{S}}_2|2M\rangle &= |2M\rangle = \lambda_2|2M\rangle,\end{aligned}$$

then, solving the system of equations (A.7) we get,

$$\hat{P}_0 = \frac{1-\hat{\boldsymbol{S}}_1\cdot\hat{\boldsymbol{S}}_2}{3}, \qquad \hat{P}_2 = \frac{\hat{\boldsymbol{S}}_1\cdot\hat{\boldsymbol{S}}_2+2}{3}, \tag{A.8}$$

and finally we can write down the interaction potential as,

$$\hat{V}(\boldsymbol{r}_1-\boldsymbol{r}_2) = \frac{4\pi\hbar^2}{m}\left(\frac{a_0+2a_2}{3} + \frac{a_2-a_0}{3}\hat{\boldsymbol{S}}_1\cdot\hat{\boldsymbol{S}}_2\right)\delta(\boldsymbol{r}_1-\boldsymbol{r}_2). \tag{A.9}$$

A.2 Second quantization

Let us define the bosonic field operator, $\psi_\alpha(\vec{r})$, which fulfill the relations,

$$\left[\psi_\alpha(\boldsymbol{r}),\psi_\beta(\boldsymbol{r}')\right] = 0, \quad \left[\psi_\alpha(\boldsymbol{r})^\dagger,\psi_\beta(\boldsymbol{r}')^\dagger\right] = 0, \quad \left[\psi_\alpha(\boldsymbol{r}),\psi_\beta(\boldsymbol{r}')^\dagger\right] = \delta_{\alpha,\beta}\delta(\boldsymbol{r}-\boldsymbol{r}'), \tag{A.10}$$

where $\alpha = -1, 0, 1$ are the spin projections, the field operator acts in the vacumm state, $|\emptyset\rangle$, as,

$$\psi_\alpha(\boldsymbol{r})|\emptyset\rangle = \sum_i \omega_i(\boldsymbol{r})|\alpha\rangle_i = \sum_i \omega_i(\boldsymbol{r})\hat{b}_{i,\alpha}|\emptyset\rangle \tag{A.11}$$

where $\omega_i(\boldsymbol{r})$ is the wannier function of the lowest Bloch band, which is a strongly localized wave function in the i-th site of the lattice, and satisfy the orthogonal relation,

$$\int d\boldsymbol{r} \quad \omega_i^*(\boldsymbol{r})\omega_j(\boldsymbol{r}) = \delta_{i,j} \tag{A.12}$$

In order to derive the model we start from the Hamiltonian for one particle which reads,

$$\hat{H} = -\frac{\hbar^2}{2m}\boldsymbol{\nabla}^2 + \hat{V}_{ext}(\boldsymbol{r}) + \hat{V}_{Int}(\boldsymbol{r}-\boldsymbol{r}') + q\hat{S}_z^2. \tag{A.13}$$

In the second quantization formalism the hopping term is

$$\begin{aligned}
\hat{H}_t &= \sum_{\alpha\beta}\int d\boldsymbol{r} \quad \psi_\alpha^\dagger(\boldsymbol{r})\langle\alpha|\left(-\frac{\hbar^2}{2m}\boldsymbol{\nabla}^2 + \hat{V}_{ext}(\boldsymbol{r})\right)|\beta\rangle\psi_\beta(\boldsymbol{r}) \\
&= \sum_{\alpha\beta}\sum_{i,j}\int d\boldsymbol{r} \quad \omega_i^*(\boldsymbol{r})\left(-\frac{\hbar^2}{2m}\boldsymbol{\nabla}^2 + \hat{V}_{ext}(\boldsymbol{r})\right)\omega_j(\boldsymbol{r})\langle\alpha|\beta\rangle\hat{b}_{\alpha,i}^\dagger\hat{b}_{\beta,i}. \\
&= -t\sum_\alpha\sum_i\left(\hat{b}_{\alpha,i}^\dagger\hat{b}_{\alpha,i+1} + \hat{b}_{\alpha,i+1}^\dagger\hat{b}_{\alpha,i}\right)
\end{aligned} \tag{A.14}$$

For the quadratic Zeeman effect we have

$$\begin{aligned}
\hat{H}_Q &= \sum_{\alpha\beta}\int d\boldsymbol{r} \quad \psi_\alpha^\dagger(\boldsymbol{r})\langle\alpha|\left(q\hat{S}_z^2\right)|\beta\rangle\psi_\beta(\boldsymbol{r}) \\
&= \sum_{\alpha\beta}\sum_{i,j} -q\int d\boldsymbol{r} \quad \omega_i^*(\boldsymbol{r})\omega_j(\boldsymbol{r})\langle\alpha|\hat{S}_z^2|\beta\rangle\hat{b}_{\alpha,i}^\dagger\hat{b}_{\beta,i}. \\
&= -Q\sum_{\alpha\beta}\sum_i\hat{b}_{\alpha,i}^\dagger[S_z^2]_{\alpha\beta}\hat{b}_{\beta,i}
\end{aligned} \tag{A.15}$$

For the interaction potential defined in equation (A.9), we get,

$$\begin{aligned}
\hat{H}_{Int} &= \frac{1}{2}\sum_{\alpha\beta\sigma\gamma}\int d\boldsymbol{r}d\boldsymbol{r}'\psi_\alpha^\dagger(\boldsymbol{r})\psi_\sigma^\dagger(\boldsymbol{r}')\langle\alpha\sigma|\left(c_0 + c_2\sum_\nu\hat{S}_\nu\otimes\hat{S}_\nu\right)\delta(\boldsymbol{r}-\boldsymbol{r}')|\gamma\beta\rangle\psi_\gamma^\dagger(\boldsymbol{r}')\psi_\beta^\dagger(\boldsymbol{r}) \\
&= \sum_i\sum_{\alpha\sigma}\frac{C_0}{2}\hat{b}_{\alpha,i}^\dagger\hat{b}_{\sigma,i}^\dagger\hat{b}_{\sigma,i}\hat{b}_{\alpha,i} + \sum_i\sum_{\alpha\beta\sigma\gamma}\frac{C_2}{2}\hat{b}_{\alpha,i}^\dagger\hat{b}_{\sigma,i}^\dagger[\hat{S}_\nu]_{\alpha\beta}[\hat{S}_\nu]_{\sigma\gamma}\hat{b}_{\gamma,i}\hat{b}_{\beta,i} \\
&= \frac{C_0}{2}\sum_i\hat{n}_i\left(\hat{n}_i - 1\right) + \frac{C_0}{2}\sum_i\left(\hat{\boldsymbol{S}}^{(i)}\cdot\hat{\boldsymbol{S}}^{(i)} - 2\hat{n}_i\right)
\end{aligned} \tag{A.16}$$

where

$$
\begin{aligned}
C_0 &= c_0 \int d\boldsymbol{r} \quad |\omega_i(\boldsymbol{r})|^4 = \frac{a_0 + 2a_2}{3} \int d\boldsymbol{r} \quad |\omega_i(\boldsymbol{r})|^4, \\
C_2 &= c_2 \int d\boldsymbol{r} \quad |\omega_i(\boldsymbol{r})|^4 = \frac{a_2 - a_0}{3} \int d\boldsymbol{r} \quad |\omega_i(\boldsymbol{r})|^4, \\
\hat{n}_i &= \sum_{\alpha} \hat{b}^{\dagger}_{\alpha,i} \hat{b}_{\alpha,i}, \\
\hat{\boldsymbol{S}}^{(i)} &= \left(\hat{S}^{(i)}_x, \hat{S}^{(i)}_y, \hat{S}^{(i)}_z \right), \\
\hat{S}^{(i)}_{\nu} &= \sum_{\alpha\beta} \hat{b}^{\dagger}_{\alpha,i} [S^{\nu}]_{\alpha\beta} \hat{b}_{\beta,i}.
\end{aligned}
$$

Finally, the Bose-Hubbard Hamiltonian for spin-1 particles, in second quantization and in the grand canonical ensemble, is given by,

$$
\begin{aligned}
\hat{H}_{HB} = -t \sum_{\alpha} \sum_{i} \left(\hat{b}^{\dagger}_{\alpha,i} \hat{b}_{\alpha,i+1} + \hat{b}^{\dagger}_{\alpha,i+1} \hat{b}_{\alpha,i} \right) - Q \sum_{i} \left(\hat{S}^{(i)}_z \right)^2 - \mu \sum_{i} \hat{n}_i \\
+ \frac{C_0}{2} \sum_{i} \hat{n}_i \left(\hat{n}_i - 1 \right) + \frac{C_0}{2} \sum_{i} \left(\hat{\boldsymbol{S}}^{(i)} \cdot \hat{\boldsymbol{S}}^{(i)} - 2\hat{n}_i \right). \quad \text{(A.17)}
\end{aligned}
$$

Appendix B

From the effective Hamiltonian to the BBH Hamiltonian

Once we get the effective matrix Hamiltonian (1.21), by means of the second order perturbation theory, we rewrite the Hamiltonian in terms of the spin-1 operators. The aim of this appendix is to present that this matrix Hamiltonian can be approximated to the bilinear biquadratic Heisenberg Hamiltonian.

The Hamiltonian for two neighboring sites can be rewritten in terms of the spin-1 operators as

$$\begin{aligned}\hat{H}_{eff} &= d_0\mathbb{1}\otimes\mathbb{1} + d_1\left(\hat{\boldsymbol{S}}\cdot\hat{\boldsymbol{S}}\right) + d_2\left(\hat{\boldsymbol{S}}\cdot\hat{\boldsymbol{S}}\right)^2 \\ &+ d_3(\hat{S}_y\hat{S}_y\otimes\hat{S}_y\hat{S}_y + \hat{S}_x\hat{S}_x\otimes\hat{S}_y\hat{S}_y + \hat{S}_y\hat{S}_y\otimes\hat{S}_x\hat{S}_x + \hat{S}_x\hat{S}_x\otimes\hat{S}_x\hat{S}_x) \\ &+ d_4\left(\hat{S}_z\hat{S}_z\otimes\hat{S}_z\hat{S}_z\right) + d_Q\left(\mathbb{1}\otimes\hat{S}_z^2 + \hat{S}_z^2\otimes\mathbb{1}\right).\end{aligned} \tag{B.1}$$

Solving the matrix equation $H^{(2)} = H_{eff}$, from (1.21) and (B.1), we determine the $\{d_i\}$ constants.

$$\begin{aligned}
d_0 &= -4t^2\left(\frac{2g_0+g_2+6Q}{3g_0g_2+2Q(2g_0+g_2)} + \frac{g_0+2g_2-6Q}{3g_0g_2-2Q(2g_0+g_2)}\right) \\
d_1 &= -\frac{2t^2}{g_2} \\
d_2 &= 2t^2\left(-\frac{1}{g_2} + \frac{g_2-g_0}{-3g_0g_2+2Q\left(2g_0+g_2\right)} + \frac{g_0-g_2}{3g_0g_2+2Q\left(g_0+2g_2\right)}+\right) \\
d_3 &= -\frac{4Qt^2\left(g_0-g_2\right)\left(3g_2\left(g_0-g_2\right)+4Q\left(g_0+2g_2\right)\right)}{g_2\left(2Q\left(g_0+2g_2\right)+3g_2g_0\right)\left(3g_0g_2-2Q\left(2g_0+g_2\right)\right)} \\
d_4 &= \frac{4Qt^2\left(g_0-g_2\right)\left(3g_2\left(g_0-g_2\right)-4Q\left(g_0+2g_2\right)\right)}{g_2\left(2Q\left(g_0+2g_2\right)+3g_2g_0\right)\left(3g_0g_2-2Q\left(2g_0+g_2\right)\right)} \\
d_Q &= \frac{4t^2\left(4Q^2\left(g_0^2-5g_2g_0-5g_2^2\right)-2g_2Q\left(g_0-g_2\right)\left(2g_0+g_2\right)+3g_0g_2^2\left(g_0+2g_2\right)\right)}{g_2\left(2Q\left(g_0+2g_2\right)+3g_2g_0\right)\left(3g_0g_2-2Q\left(2g_0+g_2\right)\right)}
\end{aligned} \tag{B.2}$$

It is presented as function of the interaction strength at each channel g_F, the QZE field Q, and the hopping energy t. Since we are considering small fields and small hopping energy, the parameter Q fulfills, $Q \sim t^2$, so that making a series expansion in t around zero, the set (B.2) is reduced to the new set given by

$$
\begin{aligned}
d_1 &= -\frac{2t^2}{g_2} + O\left[t^5\right] \\
d_2 &= \left(\frac{2}{3g_2} - \frac{4}{3g_0}\right) t^2 + \left(\frac{4}{9g_0^2} - \frac{8}{9g_0 g_2} + \frac{4}{9g_2^2}\right) t^4 + O\left[t^5\right] \\
d_3 &= \left(-\frac{4}{3g_0^2} + \frac{8}{3g_0 g_2} - \frac{4}{3g_2^2}\right) t^4 + O\left[t^5\right] \\
d_4 &= \left(\frac{4}{3g_0^2} - \frac{8}{3g_0 g_2} + \frac{4}{3g_2^2}\right) t^4 + O\left[t^5\right] \\
d_Q &= \left(\frac{4}{3g_2} + \frac{8}{3g_0}\right) t^2 + \left(-\frac{8}{9g_0^2} + \frac{16}{9g_0 g_2} - \frac{8}{9g_2^2}\right) t^4 + O\left[t^5\right].
\end{aligned}
$$

Keeping only second order contributions we can neglect the contributions of d_3 and d_4, so we can approximate the Hamiltonian to the BBH

$$
\hat{H}_{BBH} = J\left[\sum_{\langle ij\rangle} \cos\theta \hat{\mathbf{S}}_i \cdot \hat{\mathbf{S}}_j + \sum_{\langle ij\rangle} \sin\theta \left(\hat{\mathbf{S}}_i \cdot \hat{\mathbf{S}}_j\right)^2\right] - DJ \sum_i \left(\hat{S}_i^z\right)^2 \tag{B.3}
$$

where the constants are defined as,

$$
D = -\frac{Q + d_Q}{J} \qquad d_1 = J\cos\theta \qquad d_2 = J\sin\theta \tag{B.4}
$$

The Hamiltonian (B.3), is normalized to J such that the energy is measured in J units, we set $J = 1$ for simplicity. The angle θ takes values in the interval $[-\pi/2, -\pi + \arctan(1/3)]$ as the ratio g_0/g_2 varies from 0 to $-\infty$. More elaborate ideas may allow for exploring all gapped phases around the circle [48].

Appendix C

Gutzwiller approach for 2D lattice

In a two dimensional square lattice, the Gutzwiller approach becomes,

$$|\Psi\rangle = \bigotimes_{i,j} \sum_{m_{i,j}=-1}^{1} f_{m_{i,j}}^{(i,j)} |m_{i,j}\rangle, \tag{C.1}$$

where the index i goes over sites in the x-axis, and j-th goes over sites in the y-axis. Then the full set of dynamic equations for a two-dimensional square lattice is,

$$\begin{aligned}
i\hbar \frac{df_m^{i,j}}{dt} = & \frac{1}{2} J \cos\theta \sum_{m'} \Big(\Omega(m)\Omega(m') f_{m-1}^{i,j} \mathbb{F}_{m'}^{i,j}\left(m'-1\right) \\
& + \Omega(m+1)\Omega(m'+1) f_{m+1}^{i,j} \mathbb{F}_{m'}^{i,j}\left(m'+1\right) + 2mm' f_m^{i,j} \mathbb{F}_{m'}^{i,j}\left(m'\right) \Big) \\
& + \frac{1}{4} J \sin\theta \sum_{m'} \Big(\Omega(m)\Omega(m-1)\Omega(m')\Omega(m'-1) f_{m-2}^{i,j} \mathbb{F}_{m'}^{i,j}\left(m'-2\right) \\
& + \Omega(m+1)\Omega(m+2)\Omega(m'+1)\Omega(m'+2) f_{m+1}^{i,j} \mathbb{F}_{m'}^{i,j}\left(m'+1\right) \\
& + \Omega^2(m)\Omega^2(m'+1) f_m^{i,j} \mathbb{F}_{m'}^{i,j}\left(m'\right) + \Omega(m+1)\Omega(m') f_m^{i,j} \mathbb{F}_{m'}^{i,j}\left(m'\right) \\
& + 4m^2 m'^2 f_m^{i,j} \mathbb{F}_{m'}^{i,j}\left(m'\right) + 2m\Omega(m)(m'-1)\Omega(m') f_{m-1}^{i,j} \mathbb{F}_{m'}^{i,j}\left(m'-1\right) \\
& + 2m\Omega(m-1)(m'+1)\Omega(m'+1) f_{m+1}^{i,j} \mathbb{F}_{m'}^{i,j}\left(m'+1\right) \\
& + 2(m-1)\Omega(m)m'\Omega(m') f_{m-1}^{i,j} \mathbb{F}_{m'}^{i,j}\left(m'-1\right) \\
& + +2(m+1)\Omega(m+1)m'\Omega(m'+1) f_{m+1}^{i,j} \mathbb{F}_{m'}^{i,j}\left(m'+1\right) \Big) - JDm^2 f_m^{i,j}
\end{aligned} , \tag{C.2}$$

where

$$\begin{aligned}
\Omega(m) &= \sqrt{2 - m(m-1)} \\
\mathbb{F}_m^{i,j}(n) &= \left(f_n^{*i+1,j} f_m^{i+1,j} + f_n^{*i,j+1} f_m^{i,j+1} \right).
\end{aligned} \tag{C.3}$$

This equation couples the nearest sites in the x and y axis.

Bibliography

[1] Claude N. Cohen-Tannoudji. "Nobel Lecture: Manipulating atoms with photons". In: *Rev. Mod. Phys.* 70 (3 1998), pp. 707–719. DOI: 10.1103/RevModPhys.70.707. URL: https://link.aps.org/doi/10.1103/RevModPhys.70.707.

[2] Wolfgang Ketterle. "Nobel lecture: When atoms behave as waves: Bose-Einstein condensation and the atom laser". In: *Rev. Mod. Phys.* 74 (4 2002), pp. 1131–1151. DOI: 10.1103/RevModPhys.74.1131. URL: https://link.aps.org/doi/10.1103/RevModPhys.74.1131.

[3] Anna Sanpera & Veronica Ahufinger Maciej Lewenstein. *Ultracold Atoms in Optical Lattices*. Oxford University Press.

[4] Immanuel Bloch, Jean Dalibard, and Wilhelm Zwerger. "Many-body physics with ultracold gases". In: *Rev. Mod. Phys.* 80 (3 2008), pp. 885–964. DOI: 10.1103/RevModPhys.80.885. URL: https://link.aps.org/doi/10.1103/RevModPhys.80.885.

[5] K. B. Davis et al. "Bose-Einstein Condensation in a Gas of Sodium Atoms". In: *Phys. Rev. Lett.* 75.22 (1995), pp. 3969–3973. DOI: 10.1103/PhysRevLett.75.3969.

[6] M. H. Anderson et al. "Observation of Bose-Einstein Condensation in a Dilute Atomic Vapor". In: *Science* 269.5221 (1995), pp. 198–201. DOI: 10.1126/science.269.5221.198. eprint: http://www.sciencemag.org/cgi/reprint/269/5221/198.pdf. URL: http://www.sciencemag.org/cgi/content/abstract/269/5221/198.

[7] Bose. "Plancks Gesetz und Lichtquantenhypothese". In: *Zeitschrift für Physik A Hadrons and Nuclei* 26 (1 1924), pp. 178–181.

[8] A. Einstein. "Quantentheorie des einatomigen idealen Gases". In: *Sitzungsberichte der Preussischen Akademie der Wissenschaften* 3 (1925), p. 18.

[9] D. Jaksch et al. "Cold Bosonic Atoms in Optical Lattices". In: *Phys. Rev. Lett.* 81 (15 1998), pp. 3108–3111. DOI: 10.1103/PhysRevLett.81.3108. URL: https://link.aps.org/doi/10.1103/PhysRevLett.81.3108.

[10] M. Greiner et al. "Quantum phase transition from a superfluid to a Mott insulator in a gas of ultracold atoms". In: *Nature (London)* 415 (2002), p. 39. DOI: 10.1038/415039a.

[11] B. Paredes et al. "Tonks-Girardeau gas of ultracold atoms in an optical lattice". In: *Nature(London)* 429 (2004), p. 277.

[12] P. O. Fedichev et al. "Influence of Nearly Resonant Light on the Scattering Length in Low-Temperature Atomic Gases". In: *Phys. Rev. Lett.* 77 (14 1996), pp. 2913–2916. DOI: 10.1103/PhysRevLett.77.2913. URL: https://link.aps.org/doi/10.1103/PhysRevLett.77.2913.

[13] D. Jaksch and P. Zoller. "The cold atom Hubbard toolbox". In: *Annals of Physics* 315.1 (2005). Special Issue, pp. 52 –79. ISSN: 0003-4916. DOI: 10.1016/j.aop.2004.09.010. URL: http://www.sciencedirect.com/science/article/pii/S0003491604001782.

[14] D. Jaksch et al. "Entanglement of Atoms via Cold Controlled Collisions". In: *Phys. Rev. Lett.* 82 (9 1999), pp. 1975–1978. DOI: 10.1103/PhysRevLett.82.1975. URL: https://link.aps.org/doi/10.1103/PhysRevLett.82.1975.

[15] Artur Widera Tim Rom-Theodor W. Hänsch & Immanuel Bloch Olaf Mandel Markus Greiner. "Controlled collisions for multi-particle entanglement of optically trapped atoms". In: *Nature* 425 (2003), pp. 937–940. DOI: 10.1038/nature02008.

[16] Benjamin L. Brown-Jennifer Sebby-Strabley William D. Phillips & J. V. Porto Marco Anderlini Patricia J. Lee. "Controlled exchange interaction between pairs of neutral atoms in an optical lattice." In: *Nature* 448 (2007), pp. 452–456. DOI: 10.1038/nature06011.

[17] S. Fölling M. Feld-U. Schnorrberger-A. M. Rey A. Polkovnikov E. A. Demler M. D. Lukin I. Bloch S. Trotzky P. Cheinet. "Time-Resolved Observation and Control of Superexchange Interactions with Ultracold Atoms in Optical Lattices." In: *Science* 319 (2008), pp. 295–299. DOI: 10.1126/science.1150841.

[18] D.M. Stamper-Kurn H.-J. Miesner-A.P. Chikkatur W. Ketterle J. Stenger S. Inouye. "Spin domains in ground state spinor Bose-Einstein condensates". In: *Nature* 396 (1998), pp. 345–348. DOI: 10.1038/24567. URL: https://www.nature.com/articles/24567.

[19] A. J. Allen et al. "Observable vortex properties in finite-temperature Bose gases". In: *Phys. Rev. A* 87 (1 2013), p. 013630. DOI: 10.1103/PhysRevA.87.013630. URL: https://link.aps.org/doi/10.1103/PhysRevA.87.013630.

[20] Matthew P. A. Fisher et al. "Boson localization and the superfluid-insulator transition". In: *Phys. Rev. B* 40 (1 1989), pp. 546–570. DOI: 10.1103/PhysRevB.40.546. URL: https://link.aps.org/doi/10.1103/PhysRevB.40.546.

[21] Daniel S. Rokhsar and B. G. Kotliar. "Gutzwiller projection for bosons". In: *Phys. Rev. B* 44 (18 1991), pp. 10328–10332. DOI: 10.1103/PhysRevB.44.10328. URL: https://link.aps.org/doi/10.1103/PhysRevB.44.10328.

[22] Werner Krauth, Michel Caffarel, and Jean-Philippe Bouchaud. "Gutzwiller wave function for a model of strongly interacting bosons". In: *Phys. Rev. B* 45 (6 1992), pp. 3137–3140. DOI: 10.1103/PhysRevB.45.3137. URL: https://link.aps.org/doi/10.1103/PhysRevB.45.3137.

[23] M. L. Chiofalo, S. Succi, and M. P. Tosi. "Ground state of trapped interacting Bose-Einstein condensates by an explicit imaginary-time algorithm". In: *Phys. Rev. E* 62 (5 2000), pp. 7438–7444. DOI: 10.1103/PhysRevE.62.7438. URL: https://link.aps.org/doi/10.1103/PhysRevE.62.7438.

[24] L. de Forges de Parny and V. G. Rousseau. "Phase diagrams of antiferromagnetic spin-1 bosons on a square optical lattice with the quadratic Zeeman effect". In: *Phys. Rev. A* 97 (2 2018), p. 023628. DOI: 10.1103/PhysRevA.97.023628. URL: https://link.aps.org/doi/10.1103/PhysRevA.97.023628.

[25] D. M. Stamper-Kurn et al. "Optical Confinement of a Bose-Einstein Condensate". In: *Phys. Rev. Lett.* 80 (10 1998), pp. 2027–2030. DOI: 10.1103/PhysRevLett.80.2027. URL: https://link.aps.org/doi/10.1103/PhysRevLett.80.2027.

[26] M. Vengalattore et al. "Periodic spin textures in a degenerate $F = 1$ ^{87}Rb spinor Bose gas". In: *Phys. Rev. A* 81 (5 2010), p. 053612. DOI: 10.1103/PhysRevA.81.053612. URL: https://link.aps.org/doi/10.1103/PhysRevA.81.053612.

[27] S. Abe-T. Ozaki-T. Nikuni M. Shinozaki S. Tsuchiya. "Elementary Excitations of Antiferromagnetic Spin-1 Bosons in an Optical Lattice". In: *J Low Temp Phys* 175 (2014), pp. 236–242. DOI: 10.1007/s10909-013-0960-0.

[28] V. G. Bar'yakhtar et al. "Dynamics and relaxation in spin nematics". In: *Phys. Rev. B* 87 (22 2013), p. 224407. DOI: 10.1103/PhysRevB.87.224407. URL: https://link.aps.org/doi/10.1103/PhysRevB.87.224407.

[29] Adilet Imambekov, Mikhail Lukin, and Eugene Demler. "Spin-exchange interactions of spin-one bosons in optical lattices: Singlet, nematic, and dimerized phases". In: *Phys. Rev. A* 68 (6 2003), p. 063602. DOI: 10.1103/PhysRevA.68.063602. URL: https://link.aps.org/doi/10.1103/PhysRevA.68.063602.

[30] Yuki Kawaguchi and Masahito Ueda. "Spinor Bose–Einstein condensates". In: *Physics Reports* 520.5 (2012). Spinor Bose–Einstein condensates, pp. 253 –381. ISSN: 0370-1573. DOI: 10.1016/j.physrep.2012.07.005. URL: http://www.sciencedirect.com/science/article/pii/S0370157312002098.

[31] K. Rodríguez et al. "Field-Induced Phase Transitions of Repulsive Spin-1 Bosons in Optical Lattices". In: *Phys. Rev. Lett.* 106 (10 2011), p. 105302. DOI: 10.1103/PhysRevLett.106.105302. URL: https://link.aps.org/doi/10.1103/PhysRevLett.106.105302.

[32] Kei Yosida. *Theory of Magnetism*. 1st ed. Series in Solid-State Sciences. Springer-Verlag Berlin Heidelberg, 1996.

[33] Per-Olov Löwdin. "A Note on the Quantum-Mechanical Perturbation Theory". In: *The Journal of Chemical Physics* 19.11 (1951), pp. 1396–1401. DOI: 10.1063/1.1748067. eprint: https://doi.org/10.1063/1.1748067. URL: https://doi.org/10.1063/1.1748067.

[34] J. M. Luttinger and W. Kohn. "Motion of Electrons and Holes in Perturbed Periodic Fields". In: *Phys. Rev.* 97 (4 1955), pp. 869–883. DOI: 10.1103/PhysRev.97.869. URL: https://link.aps.org/doi/10.1103/PhysRev.97.869.

[35] J. H. Van Vleck. "On σ-Type Doubling and Electron Spin in the Spectra of Diatomic Molecules". In: *Phys. Rev.* 33 (4 1929), pp. 467–506. DOI: 10.1103/PhysRev.33.467. URL: https://link.aps.org/doi/10.1103/PhysRev.33.467.

[36] J. Sólyom. "Competing bilinear and biquadratic exchange couplings in spin-1 Heisenberg chains". In: *Phys. Rev. B* 36 (16 1987), pp. 8642–8648. DOI: 10.1103/PhysRevB.36.8642. URL: https://link.aps.org/doi/10.1103/PhysRevB.36.8642.

[37] U. Schollwöck, Th. Jolicœur, and T. Garel. "Onset of incommensurability at the valence-bond-solid point in the S=1 quantum spin chain". In: *Phys. Rev. B* 53 (6 1996), pp. 3304–3311. DOI: 10.1103/PhysRevB.53.3304. URL: https://link.aps.org/doi/10.1103/PhysRevB.53.3304.

[38] Andreas Mielke and Hal Tasaki. "Ferromagnetism in the Hubbard model. Examples from models with degenerate single-electron ground states". In: *Comm. Math. Phys.* 158.2 (1993), pp. 341–371. URL: https://projecteuclid.org:443/euclid.cmp/1104254245.

[39] Martin C. Gutzwiller. "Effect of Correlation on the Ferromagnetism of Transition Metals". In: *Phys. Rev. Lett.* 10 (5 1963), pp. 159–162. DOI: 10.1103/PhysRevLett.10.159. URL: https://link.aps.org/doi/10.1103/PhysRevLett.10.159.

[40] J. Hubbard and B. H. Flowers. "Electron correlations in narrow energy bands". In: *Pro. R. Soc. Lond.* 276 (1963). DOI: 10.1098/rspa.1963.0204.

[41] V. Ahufinger et al. "Disordered ultracold atomic gases in optical lattices: A case study of Fermi-Bose mixtures". In: *Phys. Rev. A* 72 (6 2005), p. 063616. DOI: 10.1103/PhysRevA.72.063616. URL: https://link.aps.org/doi/10.1103/PhysRevA.72.063616.

[42] P. W. Anderson. "The Resonating Valence Bond State in La_2CuO_4 and Superconductivity". In: *Science* 235 (1987), pp. 1196–1198. DOI: 10.1126/science.235.4793.1196.

[43] B. Edegger, V. N. Muthukumar, and C. Gros. "Gutzwiller–RVB theory of high-temperature superconductivity: Results from renormalized mean-field theory and variational Monte Carlo calculations". In: *Advances in Physics* 56.6 (2007), pp. 927–1033. DOI: 10.1080/00018730701627707.

[44] Víctor M. Pérez-García et al. "Dynamics of Bose-Einstein condensates: Variational solutions of the Gross-Pitaevskii equations". In: *Phys. Rev. A* 56 (2 1997), pp. 1424–1432. DOI: 10.1103/PhysRevA.56.1424. URL: https://link.aps.org/doi/10.1103/PhysRevA.56.1424.

[45] Víctor M. Pérez-García et al. "Low Energy Excitations of a Bose-Einstein Condensate: A Time-Dependent Variational Analysis". In: *Phys. Rev. Lett.* 77 (27 1996), pp. 5320–5323. DOI: 10.1103/PhysRevLett.77.5320. URL: https://link.aps.org/doi/10.1103/PhysRevLett.77.5320.

[46] William E. Boyce Richard C. DiPrima. *Elementary Differential Equations and Boundary Value Problems*. John Wiley & Sons.

[47] Wen-Long You, Ying-Wai Li, and Shi-Jian Gu. "Fidelity, dynamic structure factor, and susceptibility in critical phenomena". In: *Phys. Rev. E* 76 (2 2007), p. 022101. DOI: 10.1103/PhysRevE.76.022101. URL: https://link.aps.org/doi/10.1103/PhysRevE.76.022101.

[48] J. J. García-Ripoll, M. A. Martin-Delgado, and J. I. Cirac. "Implementation of Spin Hamiltonians in Optical Lattices". In: *Phys. Rev. Lett.* 93 (25 2004), p. 250405. DOI: 10.1103/PhysRevLett.93.250405. URL: https://link.aps.org/doi/10.1103/PhysRevLett.93.250405.